

# Three-flavor Collective Neutrino Oscillations on D-Wave's Advantage Quantum Annealer

Ivan A. Chernyshev,<sup>✉\*</sup>

*InQubator for Quantum Simulation (IQUS), Department of Physics,  
University of Washington, Seattle, WA 98195, USA. and*

*Theoretical Division, Los Alamos National Laboratory, Los Alamos, NM 87545, USA.*

(Dated: July 25, 2024)

In extreme environments such as core-collapse supernovae, neutron-star mergers, and the early Universe, neutrinos are dense enough that their self-interactions significantly affect, if not dominate, their flavor dynamics. In order to develop techniques for characterizing the resulting quantum entanglement, I present the results of simulations of Dirac neutrino-neutrino interactions that include all three physical neutrino flavors and were performed on D-Wave Inc.'s **Advantage** 5000+ qubit quantum annealer. These results are checked against those from exact classical simulations, which are also used to compare the Dirac neutrino-neutrino interactions to neutrino-antineutrino and Majorana neutrino-neutrino interactions. The D-Wave **Advantage** annealer is shown to be able to reproduce time evolution with the precision of a classical machine for small numbers of neutrinos and to do so without Trotter errors. However, it suffers from poor scaling in qubit-count with the number of neutrinos. Two approaches to improving the qubit-scaling are discussed, but only one of the two shows promise.

## I. INTRODUCTION

In extreme-density and extreme-temperature environments, such as core-collapse supernovae (CCSNe), neutron-star mergers and the early Universe, neutrinos dominate the transport of energy, momentum, entropy, neutron-to-proton ratios, and lepton flavor composition, among other characteristics (for recent reviews, see Refs. [1–5]). Several neutron star merger studies show neutrinos having an effect in phenomena such as mass ejection and accretion, as well as gamma-ray burst formation [6–8]. In CCSNe, neutrinos carry away 99% of the gravitational binding energy released by the collapse of the iron core at the supernova's beginning [9–19]. There is also a consensus in the field that these neutrinos are the primary triggering mechanism in most CCSNe [9, 20–26]. Neutrinos are also thought to play a key role in nucleosynthesis in all three of the above phenomena, with a few light isotopes and several heavy ones being particularly dependent on neutrino processes [27–34].

One challenge is that at such high densities and temperatures, neutrino-neutrino interactions, which manifest as collective neutrino oscillations, are significant enough to produce macroscopic effects. Recent simulations have shown that a few neutrino-dependent processes which are theorized to be critical in the nucleosynthesis of nuclei with mass numbers above 64 are heavily dependent on collective neutrino oscillations [29, 35, 36]. Collective neutrino oscillations are also expected to have an effect on r-process, which is responsible for half of the abundance of elements in the Universe heavier than iron [37]. In short, collective neutrino oscillations must be taken into account in order to fully understand the dynamics of neutrinos in high-temperature, high-density astrophysical phenomena.

Collective neutrino oscillations are a highly nonlinear many-body problem [38–40]. One commonly-used method for highly nonlinear many-body problems is mean-field theory, which treats all but the observed neutrino as a single-valued background interacting with said neutrino [41]. This approach is effective in achieving a linear scaling of computational resources with the number of modes in the neutrino-state-space considered in the simulation. This is typically sufficient for studies at the astrophysical scale to take place. However, it is unable to simulate quantum entanglement and incoherent scattering. Whether this fact invalidates the use of mean-field theory in macroscopic neutrino systems is still an unanswered question [42].

Meanwhile, methods that do account for entanglement in collective neutrino oscillations have been utilized extensively. They include exact time evolution through numerical integration or diagonalization of the Hamiltonian or the equations of motion, the Bethe ansatz, and tensor network algorithms [43–63]. For

---

\* ivanc3@uw.edu

neutrino systems so dense that neutrino-neutrino interaction is the only term that needs to be considered, generalized angular momentum representations can be used to simulate up to  $O(10^6)$  neutrinos [64–68]. However, as is the case with many simulations of quantum-mechanical phenomena, the resources needed to study entanglement in collective neutrino oscillations on classical computers scale exponentially with the size of the system in the general case [36, 55, 69–72]. As a result, simulations of collective neutrino oscillations using exact numerical methods have been limited to up to 20 neutrinos. Tensor network [54–56] and matrix product state methods [44, 73, 74], which are two of the leading methods of approximate simulation of quantum mechanical systems, can simulate considerably more neutrinos. For instance, the time-dependent variational principle (TDVP) can currently be used to simulate up to approximately 50 neutrinos if the neutrinos start in the same flavor, though performance has been found to be little better at scale than exact simulations for a mix of initial flavors [56].

In the end, the fundamental problem of exponential scaling of computational resource requirements with system size has not been solved for simulations that utilize state-of-the-art computers. This presents an opportunity for quantum computers to produce an advantage, as they are capable of efficiently representing any local quantum system [75, 76]. Simulations of two-flavor collective neutrino oscillations have been done on devices such as Quantinuum’s trapped ion devices [77, 78], IBM’s superconducting devices [70, 79, 80], and D-Wave’s **Advantage** quantum annealer [81]. For a recent review of the entire field of collective neutrino oscillations, see Ref. [71].

The above literature has only studied neutrinos under the assumption that the number of possible neutrino flavors,  $n_f$ , is 2, with the physical  $n_f = 3$  collective neutrino oscillation picture being analyzed entirely in the classical approximation and in mean-field theory [35, 59, 60, 82–90] until 2023, when the first exact calculations of three-flavor collective neutrino oscillations were done [69, 72]. Ref. [72] found a difference between results for  $n_f = 3$  and those for  $n_f = 2$ . One of the limitations of the first two exact  $n_f = 3$  studies was that they used the single-angle approximation. Physically, neutrino-neutrino interactions depend on the angle between the trajectories of the interacting neutrinos. However, in the single-angle approximation, the trajectory-directions are averaged over [91]. Supernova models that use the single-angle approximation exhibit several differences with those that do not [92–96]. For instance, the single-angle approximation produces collective neutrino oscillations at earlier times than the full (“multi-angle”) treatment of each neutrino’s trajectory [97]. These differences reflect themselves in supernova neutrino spectra [35, 85, 98–101] and in nucleosynthesis [37].

Thus, it is important to the astrophysical applications of neutrino science to devise techniques for multi-angle simulations of collective neutrino oscillations with  $n_f = 3$ , and to create algorithms by which future quantum computers can efficiently compute such simulations. This paper details the extension of the two-flavor collective neutrino oscillation analysis in Ref. [81] to three flavors. The number of neutrinos in the simulation,  $N$ , is set to 2 for tests and simple demonstrations and 4 for the main run. While such system sizes are microscopic compared to what is possible with mean-field theory and are too small to have direct applications to astrophysical observables or supernova thermodynamics, they can still provide insight into the entanglement structure evolution of dense neutrino systems and are comparable to the  $N = 5$  choice in the exact  $n_f = 3$  simulations that have been done so far [69, 72]. Furthermore, system sizes of this scale allow for testing of quantum algorithms that will enable the macroscopic simulation of full neutrino entanglement dynamics once quantum devices with sufficient qubit-count and state fidelity become available.

This paper is organized as follows. In Section II, the Hamiltonian that defines the dynamics of the collective neutrino oscillations is established and discussed. In Section III, the techniques for implementing dynamics on D-Wave’s **Advantage** quantum annealer are described. Section IV presents the results of the simulation. Section V covers attempts to obtain scaling quantum advantage on a quantum annealer. Section VI discusses extension of the study to antineutrinos, Majorana neutrinos, and to time-dependent neutrino-neutrino interactions. Section VII discusses the implications of the results and future directions of research. Appendices discuss technical details.

## II. COLLECTIVE NEUTRINO OSCILLATION HAMILTONIAN

The terms relevant to the construction of a Hamiltonian describing the flavor dynamics of collective neutrino oscillations are the vacuum propagation (which effects neutrino oscillations), the neutrino-neutrino interactions [38–40], and the matter term (notably the Mikheyev-Smirnov-Wolfenstein (MSW) effect [102–104]). Following the leads of Refs. [45, 48, 51–53, 56, 72, 105–107] the matter effects are assumed to be

negligible. Studies implementing a co-rotating frame have supported this approximation for the case of homogeneous systems modeled with the mean-field theory approach [108, 109]. The neutrino-neutrino terms are dependent on neutrino density [110] and hence are time-dependent in physical applications, as neutrinos radiate outward from a source and their density decreases as they do so. However, one of the primary aims of this study is to devise techniques for simulation on the **Advantage** quantum annealer. For this reason, the Hamiltonian is treated as time-independent, following the lead of Ref. [81]. Additionally, only coherent interactions that either preserve or exchange the neutrino momenta (“coherent elastic forward scattering”) are taken into account. Discussion in the literature of interactions other than coherent elastic forward scattering has been taking place for decades [45, 48, 50, 54–56, 58, 64, 66–68, 105, 111–120]. While the first quantum many-body study of collective neutrino oscillations that included the full forward and non-forward scattering was recently done [61], in this work the coherent forward scattering approximation is used, in the interest of a simple mapping of the problem onto quantum devices.

$n_f = 3$  collective neutrino oscillations of  $N$  neutrinos in the mass basis can be represented in terms of the Gell-Mann matrices [72, 117]:

$$H_{CNO} = \sum_{p=1}^N \vec{B} \cdot \vec{\lambda}_p + \sum_{p=1}^{N-1} \sum_{p'=p+1}^N k(1 - \cos \theta_{pp'}) \vec{\lambda}_p \cdot \vec{\lambda}_{p'} \quad (1)$$

where  $\vec{\lambda}_p$  is the 8-term vector composed of the Gell-Mann matrices applied to the neutrino indexed by  $p$ ,  $\theta_{pp'}$  is the angle between the momenta of the neutrinos indexed by  $p$  and  $p'$ ,  $k$  is the coupling strength of the neutrino-neutrino interaction,  $E$  is the energy of the neutrino in question, and  $\vec{B}$  is a vector that creates the diagonalized single-neutrino oscillation term when dotted with  $\vec{\lambda}_p$ . The diagonalized single-vector neutrino oscillation term is determined by two parameters:  $\delta m^2$ , the difference in mass-squared between the first and second mass eigenstates, and  $\Delta m^2$ , the difference between the third mass eigenstate’s mass-squared and the mean of the masses-squared of the first and second mass eigenstates (following the convention of Ref. [121]). Normal mass hierarchy is assumed throughout this work. It turns out that two neutrinos with the same starting state and with the same momentum behave exactly the same as if they were just one neutrino. Hence, following the lead of Ref. [72], a neutrino referenced by  $p$  can be thought of as a momentum-mode. In order to convert between the flavor and mass basis, the PMNS matrix [122–124] is utilized:

$$U_{PMNS} = \begin{pmatrix} 1 & 0 & 0 \\ 0 & c_{23} & s_{23} \\ 0 & -s_{23} & c_{23} \end{pmatrix} \begin{pmatrix} c_{13} & 0 & s_{13}e^{-i\delta} \\ 0 & 1 & 0 \\ -s_{13}e^{i\delta} & 0 & c_{13} \end{pmatrix} \begin{pmatrix} c_{12} & s_{12} & 0 \\ -s_{12} & c_{12} & 0 \\ 0 & 0 & 1 \end{pmatrix} \quad (2)$$

where  $c_{ij} = \cos \theta_{ij}$  and  $s_{ij} = \sin \theta_{ij}$ . One feature of Eq. 1 is that as long as the absolute values of the neutrino energies are all the same, the single-neutrino term commutes with the neutrino-neutrino interaction term. Related to this, the neutrino-neutrino interaction term is independent of the basis that the neutrinos are in, so long as the neutrinos are all in the same basis. This fact enables the strategy utilized in Sec. IV to work and has several consequences for the observations therein.

The parameters used in this project can be found in Tab. I. The single-neutrino term parameters are drawn from Ref. [72] and fall within the  $1 \sigma$  confidence interval of experimental results if rounded to three significant figures as of the release of the 2023 PDG Review [125]. For  $N = 4$ , the angles  $\theta_{ij}$  between the neutrinos, used for the neutrino-neutrino interaction term, are given by the anisotropic angle distribution from Ref. [81], with  $\xi = 0.9$ :

$$\theta_{ij} = \arccos(\xi) \frac{|i - j|}{N - 1} \quad (3)$$

### III. IMPLEMENTATION ON D-WAVE ADVANTAGE QUANTUM ANNEALER

D-Wave’s **Advantage** quantum annealer is a 5000+-qubit device [126] designed with the express function of obtaining the ground state of a user-specified classical Ising model through a procedure known as quantum

Parameter	Values	PDG Experimental results
$E_i$	$10^7$ eV	n/a
$\delta m^2$	$7.42 * 10^{-5}$ eV	$(7.53(18)) * 10^{-5}$ eV
$\Delta m^2$	$2.44 * 10^{-3}$ eV	$(2.475(33)) * 10^{-3}$ eV
$\theta_{\nu 12}$	0.591667	0.587(14)
$\theta_{\nu 13}$	0.148702	0.1489(24)
$\theta_{\nu 23}$	0.840027	$0.832^{(+18)}_{(-12)}$
$\delta$	4.36681	3.86(66)
$\theta_{12}$ (N = 2)	$\frac{\pi}{4}$	n/a
$\theta_{ij}$ (N = 4)	Eq. 3	n/a
$k$	$1.75 * 10^{-12}$	n/a

TABLE I. The parameters used in the exact simulation of  $n_f = 3$  interacting neutrino systems described by Eq. 1 as well as the experimental results from the 2023 PDG Review [125] for neutrino oscillation terms. For all  $n_f = 2$  studies, unless otherwise stated, the mass-difference is set to  $\Delta m^2$  and the mixing angle to  $\theta_{\nu 12}$ . Normal mass hierarchy is assumed.

annealing. In quantum annealing, the system begins in the ground state of one Hamiltonian  $H_i$  and is time-evolved on a Hamiltonian  $H_a$  that begins as  $H_i$  but gradually becomes a different Hamiltonian,  $H_f$ . As long as  $H_a$ 's transition from  $H_i$  to  $H_f$  is sufficiently slow, the system's final state will be the ground state of  $H_f$  [127]. For **Advantage**,  $H_i = (\sum_i \hat{\sigma}_x^{(i)})$  and  $H_f = (\sum_i h_i \hat{\sigma}_z^{(i)} + \sum_{i>j} J_{ij} \hat{\sigma}_z^{(i)} \hat{\sigma}_z^{(j)})$ , where  $\hat{\sigma}_x^{(i)}$  and  $\hat{\sigma}_z^{(i)}$  are the Pauli-x and Pauli-z matrices, respectively, acting on the  $i^{th}$  qubit, and  $h_i$  and  $J_{ij}$  are the user-tunable parameters. In turn,  $H_a$  is set to the following Hamiltonian [128]:

$$H_{ising} = \frac{A(s)}{2} (\sum_i \hat{\sigma}_x^{(i)}) + \frac{B(s)}{2} (\sum_i h_i \hat{\sigma}_z^{(i)} + \sum_{i>j} J_{ij} \hat{\sigma}_z^{(i)} \hat{\sigma}_z^{(j)}) \quad (4)$$

where A(s) and B(s) are time-dependent parameters. s is a time-parameter, defined as  $s = t/t_f$ , where t is time and  $t_f$  is the total time of the anneal. In order for quantum annealing to be executed, A(s) and B(s) are defined so that  $A(0) \gg B(0)$  and  $A(1) \ll B(1)$ . The exact definitions of A(s) and B(s) are known as the annealing schedule.

One of the main documentation-prescribed methods of mapping an optimization problem onto **Advantage** is to map it onto a QUBO (quadratic unconstrained binary optimization) problem [126, 128, 129]. A QUBO problem is one that involves the minimization of a function of the form

$$f(x) = \sum_i Q_{ii} \mathbf{x}_i + \sum_{i<j} Q_{ij} \mathbf{x}_i \mathbf{x}_j \quad (5)$$

with  $\mathbf{x}_i$  being a binary variable with 2 possible values: 0 or 1.

QUBO problems are directly mappable onto **Advantage**'s  $H_f$  [126] and one can directly submit a problem with a given set of  $Q_{ij}$  values to the Ocean interface provided by DWave Systems, which will convert it to a set of  $h_i$  and  $J_{ij}$  parameters to be submitted directly to the annealer [128].

**Advantage**'s hardware runs on an architecture known as Chimaera. This means that the two-qubit couplings  $J_{ij}$  can act between any qubit and one of the 15 other qubits on **Advantage** that Chimaera connects it to [126]. However, collective neutrino oscillations require coupling between all pairs of simulated neutrinos. The required all-to-all coupling is obtained on **Advantage** through a process called minor-embedding. Minor-embedding works by mapping each logical qubit to a set of physical qubits called a "chain". All qubits in a chain are fixed to the same value by setting the  $Q_{ij}$  parameters between them to a negative value high enough in magnitude (which is called the "chain-strength") to do so and that is set by the user [128]. In this project, the chain-strength is set to 1, because it is high enough to prevent almost all differences in value between qubits in a chain ("chain-breaks"), and higher values have been found to interfere with convergence to the final ground state. Because all of the qubits in a chain are the same value, the chains can be treated as 1 qubit with a connectivity equal to the sum of the connectivities of the qubits minus the number of connections between qubits on the same chain. In this project, D-Wave's provided minor-embedders, which have a quadratic complexity [128], are used for this purpose.

### A. Mapping time evolution onto a QUBO problem

Time-evolution is encoded in an annealer through a Feynman clock Hamiltonian [130]:

$$C = C_0 + \frac{1}{2} \sum_t (I \otimes |t\rangle \langle t| - U_t \otimes |t+dt\rangle \langle t| - U_t^\dagger \otimes |t+dt\rangle \langle t| + I \otimes |t+dt\rangle \langle t+dt|) \quad (6)$$

In the Feynman clock Hamiltonian approach, the time-evolution is discretized into time-steps separated by increment  $dt$ . One register of states is assigned to each time-step and represents the system at that time-step. The Hamiltonian itself is designed so that the penalty term,  $C_0 = (I - |\Psi_0\rangle \langle \Psi_0|) \otimes |0\rangle \langle 0|$ , ensures that the desired initial state  $|\Psi_0\rangle$  is the ground state of the initial time register and the other terms ensure that the ground state of each of the other registers is equivalent to the result of applying the time-evolution operator,  $U_t = e^{-iHdt}$ , to the state on the previous time-step's register.

The matrix form of the Feynman clock Hamiltonian is digitized (with a register of  $K$  qubits representing each state-amplitude) in order to map it to a QUBO problem. The digitization, following the lead of Refs [81, 131], works as follows:

$$a_\alpha = -2q_K^\alpha + \sum_{i=1}^{K-1} \frac{q_i^\alpha}{2^{K-i}} \quad (7)$$

with  $a_\alpha$  being the  $\alpha^{th}$  element of the original state-vector  $a$  and the  $q_i^\alpha$  is the  $i^{th}$  digit in the digitization of  $a_\alpha$ . Each  $q_i^\alpha$  can be either 0 or 1 when measured.  $K$  is a digitization parameter that denotes the precision at which to truncate the digitization. If one works in a basis where the Hamiltonian submitted to the annealer is real, then one can simply apply the digitization to the said Hamiltonian and it would be ready to submit to the annealer. However, the Feynman clock Hamiltonian by default is complex, and so must be mapped to a real matrix so that it is submittable as a QUBO model. This is done using the method used in Refs. [81, 132]. The size of the statevector-space is doubled, and half of the result is delegated to the real component and the other half to the imaginary component. The resulting breakdown of the Feynman clock Hamiltonian is as follows:

$$\bar{a}_\alpha a_\beta C_{\alpha\beta} = \bar{a}_\alpha^{Re} a_\beta^{Re} C_{\alpha\beta}^{Re} - \bar{a}_\alpha^{Re} a_\beta^{Im} C_{\alpha\beta}^{Im} + \bar{a}_\alpha^{Im} a_\beta^{Re} C_{\alpha\beta}^{Im} + \bar{a}_\alpha^{Im} a_\beta^{Im} C_{\alpha\beta}^{Re} \quad (8)$$

Combining Eq. 7 and 8 leads us to

$$Q_{\alpha,i;\beta,j} = \begin{cases} 2^{i+j-2K} (-1)^{\delta_{iK}+\delta_{jK}} C_{\alpha\beta}^{Re}, & \text{if } 1 \leq i, j \leq K, \\ -2^{i+j'-2K} (-1)^{\delta_{iK}+\delta_{j'K}} C_{\alpha\beta}^{Im}, & \text{if } 1 \leq i, j' \leq K, \\ 2^{i'+j-2K} (-1)^{\delta_{i'K}+\delta_{jK}} C_{\alpha\beta}^{Im}, & \text{if } 1 \leq i', j \leq K, \\ 2^{i'+j'-2K} (-1)^{\delta_{i'K}+\delta_{j'K}} C_{\alpha\beta}^{Re}, & \text{if } 1 \leq i', j' \leq K. \end{cases} \quad (9)$$

where  $Q_{\alpha,i;\beta,j}$  is a QUBO matrix standing in for the Feynman clock Hamiltonian, with  $\alpha$  and  $\beta$  standing in for statevector indices and  $i$  and  $j$  standing for elements in the digitization. Note that  $i' = i - K$  and  $j' = j - K$  are indices that are in play to represent the extra space allocated to represent the statevector's imaginary component.

One method of improving the results obtainable from a quantum annealer is AQAE (adaptive quantum annealing eigensolver). AQAE works by doing the anneal process multiple times (or "zoom-steps"), with each anneal being a correction from the previous anneal with a finer digitization, and was implemented by Refs. [81, 133, 134]. For the statevectors, the resulting digitization at a given zoom-step is

$$a_\alpha^{z+1} = a_\alpha^z - 2^{-z} q_K^\alpha + \sum_{i=1}^{K-1} \frac{q_i^\alpha}{2^{K-i+z}} \quad (10)$$

and for the QUBO matrix, it is

$$Q_{\alpha,i;\beta,j} = \begin{cases} 2^{i+j-2K-2z} (-1)^{\delta_{iK}+\delta_{jK}} C_{\alpha\beta}^{Re} \\ + 2\delta_{\alpha\beta}\delta_{ij} 2^{(i-K-z)} (-1)^{\delta_{iK}} \sum_{\gamma} (a_{\alpha}^{Re,(z)} C_{\alpha\beta}^{Re} + a_{\alpha}^{Im,(z)} C_{\alpha\beta}^{Im}), & \text{if } 1 \leq i, j \leq K, \\ -2^{i+j'-2K-2z} (-1)^{\delta_{iK}+\delta_{j'K}} C_{\alpha\beta}^{Im}, & \text{if } 1 \leq i, j' \leq K, \\ 2^{i'+j-2K-2z} (-1)^{\delta_{i'K}+\delta_{jK}} C_{\alpha\beta}^{Im}, & \text{if } 1 \leq i', j \leq K, \\ 2^{i'+j'-2K-2z} (-1)^{\delta_{i'K}+\delta_{j'K}} C_{\alpha\beta}^{Re} \\ + 2\delta_{\alpha\beta}\delta_{i'j'} 2^{(i'-K-z)} (-1)^{\delta_{i'K}} \sum_{\gamma} (a_{\alpha}^{Im,(z)} C_{\alpha\beta}^{Re} - a_{\alpha}^{Re,(z)} C_{\alpha\beta}^{Im}), & \text{if } 1 \leq i', j' \leq K. \end{cases} \quad (11)$$

Here,  $z$  denotes the number of zoom-steps done so far in the AQAE process. The method above is theoretically capable of annealing to the desired target state with the minimal possible overhead available to **Advantage**. However, it is vulnerable to getting stuck at local minima if the noise is too high in magnitude. To remedy this, several measures are taken. First, the penalty terms are set to the maximum-magnitude  $h_i$  values that would achieve the desired initial state. Additionally,  $a_{\alpha}^0$  is set to the initial state for the  $t = 0$  register and to all  $|0\rangle$ 's for the evolved-state registers, so that all updates to the initial state are fixed to the zero-state. This minimizes the probability of the wrong initial state and thus removes one of the main sources of error for the annealer. Second, each zoom-step is repeated once with the signs of the updates in the digitization in Eq. 10 being flipped. The resulting digitization is as follows:

$$a_{\alpha}^{z+1} = a_{\alpha}^z + 2^{-z} q_K^{\alpha} - \sum_{i=1}^{K-1} \frac{q_i^{\alpha}}{2^{K-i+z}} \quad (12)$$

This provides a positive counterpart to the dominant negative term in the digitization. The main benefit of this is that an error in said dominant term can be compensated for by one qubit rather than requiring the rest of the register. This greatly widens the margin for individual qubit error and allows for system sizes up to the maximum size simulated in this project to converge despite the noise on the devices. Additionally, this allows  $K = 1$  simulations to be feasible. In Ref. [81],  $K = 1$  simulations failed to converge partially due to only -1 and 0 values being representable on the qubit-registers. This is no longer a problem with the extra reverse-digitization step. In App. B, a full test of this process on both **neal**, DWave, Inc.'s provided classical thermal annealer, and on the **Advantage** annealer for a two-neutrino system is discussed.

One limitation of AQAE is that it cannot obtain quantum advantage for time evolution. This is because its construction of the QUBO matrix submitted to the device at each iteration involves the matrix-multiplication of the state-vector obtained from the previous iteration, which is a task of equal computational difficulty to classically obtaining the time-evolution. AQAE will nonetheless be necessary as long as quantum annealers lack the capability to precisely digitize even the least precise systems, so that algorithms for when such capabilities exist can be created.

#### IV. N = 4 TIME EVOLUTION SIMULATIONS

A system's neutrino-count  $N$  must be at least 3 in order to capture the physical differences between neutrino-neutrino interactions in the case where the number of flavors,  $n_f$ , is 2 and those in the case where  $n_f = 3$ . However, time-evolution of systems with 30 basis-states failed to converge on **Advantage**. 20 basis-state systems mostly annealed like normal but did have a noticeably higher frequency stuck at a local minimum before convergence. This presents a challenge, because the Hilbert-space size of a system with  $N = 3$  and  $n_f = 3$  is 27, which is within the range at which the time-evolution fails to reach convergence on the annealer.

To circumvent this, domain-decomposition is used. This technique, which has been used in applications of the quantum annealer to finding the ground state of non-Abelian quantum field theories [134, 135], takes advantage of the block-diagonalized structure of Hamiltonians to find the solution for each block separately. The mass-basis collective neutrino oscillation Hamiltonian is natively block-diagonalized: it doesn't change the number of neutrinos in each mass-eigenstate. An  $N = 5$ ,  $n_f = 3$  system could be encoded onto **Advantage** in this way, but could not be simulated because the largest subsystem produced in this case would be a 30-state space.

Hence, this technique was used to find the time-evolution of the quantum entanglement of an  $n_f = 3$ ,  $N = 4$  system with an initial state of  $|\nu_e\nu_e\nu_{\tau}\nu_{\mu}\rangle$ . The motivation for finding the entanglement is that

entanglement is the quantity which indicates intractability with classical devices [44, 136–139]. This system is analogous to the  $|\nu_e\nu_e\nu_\mu\nu_\mu\rangle$  initial state used for the  $n_f = 2$ ,  $N = 4$  simulation in Ref. [81]. The third neutrino in the system, which for an initial state of  $|\nu_e\nu_e\nu_\mu\nu_\mu\rangle$  is the neutrino starting out in the  $\nu_\tau$  state, is treated as a probe interacting with a system of  $\nu_e$  and  $\nu_\mu$ . Since (as discussed in Sec. II), Eq. 1 commutes for systems where all neutrinos have the same energy magnitude, it seems intuitive that the single-neutrino oscillation term has no effect on the entanglement witnesses. This is because due to the commutation, all of the time-evolution from the single-neutrino oscillation can be pushed to the end of the time-evolution, where it would have no effect on the entanglement, and ostensibly, the entanglement witnesses as well. While this study was unable to find a proof of this fact in general, the time-evolution of the entanglement witnesses of an  $n_f=3$ ,  $N = 4$  neutrino system was repeated for four different choices of  $\vec{B}$ . These were:

- $\vec{B} = (0, 0, 0, 0, 0, 0, 0)$ , i.e. no single-neutrino flavor oscillation
- $\vec{B} = (0, 0, -\frac{\delta m^2}{4E}, 0, 0, 0, -\frac{\Delta m^2}{2\sqrt{3}E})$ , from the derivation of the ultrarelativistic-limit time-evolution of a generic three-mass-eigenstate system in App. A
- $\vec{B} = (0, 0, -\frac{\delta m^2}{12E}, 0, 0, 0, -\frac{\Delta m^2}{6\sqrt{3}E})$
- $\vec{B} = (0, 0, -\frac{\delta m^2}{4E}, 0, 0, 0, -\frac{\Delta m^2}{4E})$ , from Ref. [71]

There was no difference found between the results produced on classical devices for the above four choices of  $\vec{B}$ . Hence, for purposes of Sec. IV, I will treat the choice of  $\vec{B}$  as arbitrary. If  $\vec{B}$  is not treated as arbitrary, it is straightforward to simulate systems where momentum magnitudes vary between neutrinos. However, in this study the momentum magnitudes are fixed to the same value in order to compare to the results in Ref. [81]. The Hamiltonian parameters can be found in Tab. I.

The first step was the simulation of the system using exact classical numerical methods and comparison to results in the case the neutrino oscillation parameters in Tab. I were zeroed out one by one, as well as to analogous simulations for initial states of  $|\nu_e\nu_e\nu_\mu\nu_\mu\rangle$  and  $|\nu_e\nu_e\nu_e\nu_\mu\rangle$ . Additionally, the classical simulations for  $|\nu_e\nu_e\nu_\mu\nu_\mu\rangle$  were repeated with a Hamiltonian for  $n_f = 2$  that in the mass-basis works out to [81],

$$H_{CNO}(n_f = 2) = \sum_{p=1}^N \vec{B}_{2p} \cdot \vec{\sigma}_p^z + \sum_{p=1}^{N-1} \sum_{p'=p+1}^N k(1 - \cos \theta_{pp'}) \vec{\sigma}_p \cdot \vec{\sigma}_{p'} \quad (13)$$

where  $\vec{B}_{2p}$  is a 3-component vector that effects the collective neutrino oscillation and  $\vec{\sigma}_p = (\hat{\sigma}_p^x, \hat{\sigma}_p^y, \hat{\sigma}_p^z)$ , where  $\hat{\sigma}_p^x$ ,  $\hat{\sigma}_p^y$ , and  $\hat{\sigma}_p^z$  are the Pauli-x, Pauli-y, and Pauli-z operators, respectively, acting on the  $p^{th}$  neutrino. The entanglement entropy of each neutrino and the negativity between each pair of neutrinos was then extracted for each sample. The entanglement entropy, which is a measure of entanglement between a given neutrino (labeled with index  $i$ ) and all other neutrinos, is calculated as a von Neumann entropy [140]:

$$S_i(t) = -Tr(\rho_i \log_2(\rho_i)) \quad (14)$$

where  $\rho_i$  is the one-neutrino reduced density matrix for the  $i^{th}$  neutrino. The logarithmic negativity, which is a measure of entanglement between two specific neutrinos (labeled with indices  $i$  and  $j$  in this case) is calculated like so [141, 142]:

$$N_{ij}(t) = \log_2 \|\rho_{ij}^\Gamma(t)\|_1 \quad (15)$$

where  $\rho_{ij}$  is the reduced density matrix for the  $ij$  neutrino pair,  $\Gamma$  indicates partial transposition of the matrix it is a superscript of, and  $\|\cdot\|_1$  is the trace norm.

As mentioned above, the values of the single-neutrino oscillation parameters did not affect the behavior of the entanglement witnesses. Additionally the results for an initial state of  $|\nu_e\nu_e\nu_\mu\nu_\mu\rangle$  were the same for  $n_f = 2$  and  $n_f = 3$ . Hence, the only differences found were based on the initial state, specifically where there are 3 flavors in the initial state. The results for the probe-neutrino's entanglement entropy and negativities with each other neutrino are shown in Fig. 1. Generally, the results for each initial state were distinct, but

there were a few highlights. First, the probe’s entanglement entropy exhibits a similar peak for an initial state of  $|\nu_e\nu_e\nu_\tau\nu_\mu\rangle$  as for an initial state of  $|\nu_e\nu_e\nu_e\nu_\mu\rangle$ , though at a higher magnitude, reflecting the fact that the maximum magnitude of entanglement entropy is  $\log_2(3)$  for  $n_f = 3$  and 1 for  $n_f = 2$ . The negativities for the  $|\nu_e\nu_e\nu_\tau\nu_\mu\rangle$  seemed to exhibit the peaks of both the negativities of  $|\nu_e\nu_e\nu_\mu\nu_\mu\rangle$  and the negativities of  $|\nu_e\nu_e\nu_e\nu_\mu\rangle$ . Although this result is pretty abstract, it nonetheless suggests a degree of unique behavior from the introduction of a third flavor into an interacting neutrino system.

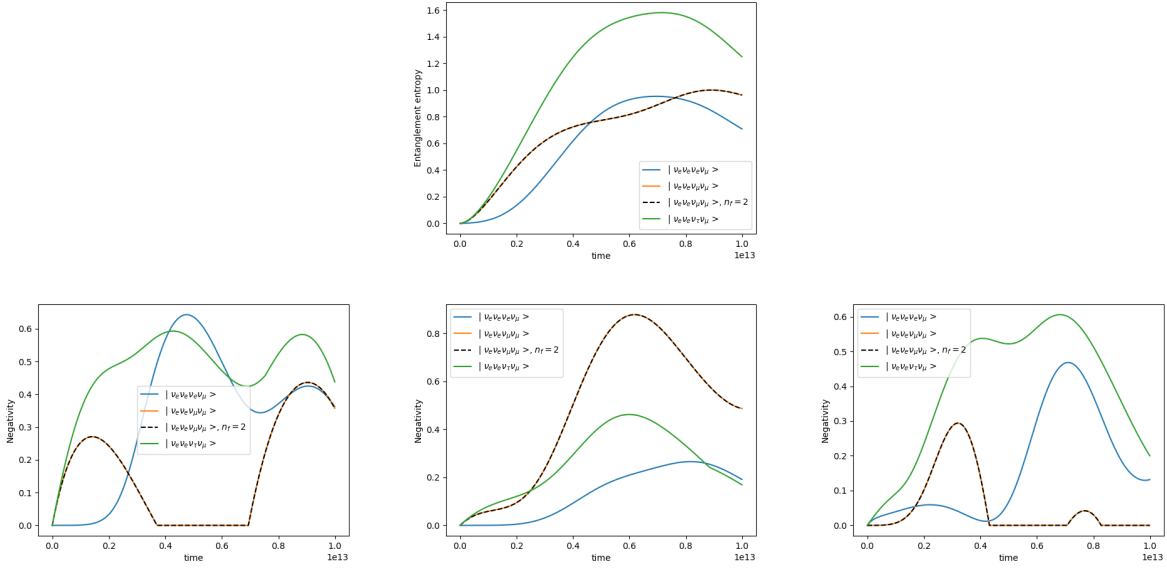


FIG. 1. Under collective neutrino oscillations, time evolution of: entanglement entropy of the third neutrino (top), negativity between neutrinos 1 and 3 (bottom left), negativity between neutrinos 2 and 3 (bottom middle), and negativity between neutrinos 3 and 4 (bottom right). The terms in the  $\nu$ - $\nu$  interaction term of the Hamiltonian are given by Tab. I. Number of neutrinos in the simulation,  $N$ , is 4 and number of neutrino-flavors,  $n_f$ , is 3. The purple icon at the top-right indicates exact simulation on a classical device [143].

The results for an initial state of  $|\nu_e\nu_e\nu_\tau\nu_\mu\rangle$  with Hamiltonian parameters in Tab. I were replicated on **Advantage**. Nine different times were sampled, and the following procedure was used for each time: The initial state would be transformed into the mass-basis and split into blocks, each of which is composed of all mass-basis states with a given number of neutrinos in each mass-basis eigenstate. For  $N = 4$  and  $n_f = 3$ , there are 3 blocks of size 1, 6 blocks of size 4, 3 blocks of size 6, and 3 blocks of size 12. Time-evolution using the techniques outlined in Sec. III would be done separately for each block. In the event of a nonconvergence, defined as the previous 8 iterations achieving a percentage difference of less than 1% between the expectation values of the Feynman clock Hamiltonian obtained from Eq. 11 from adjacent iterations, the digitization would be rewound to the last iteration at which the progression of the Feynman clock expectation value was consistent with that of converging samples and would begin again from that point. The results from each block would be put back together to form the result for the state-vector, from which the entanglement entropy and negativity would then be extracted. The results for the “probe” third neutrino are seen in Fig. 2. All results are enumerated in App. C. Successful convergence to the classical result was achieved on **Advantage** to classical machine precision without Trotter error, similar to what was accomplished in Ref. [81]. In addition, the natural block-diagonalization of the neutrino mass basis was demonstrated to be a promising avenue for extending the reach of quantum simulation of  $\nu$ - $\nu$  interaction.



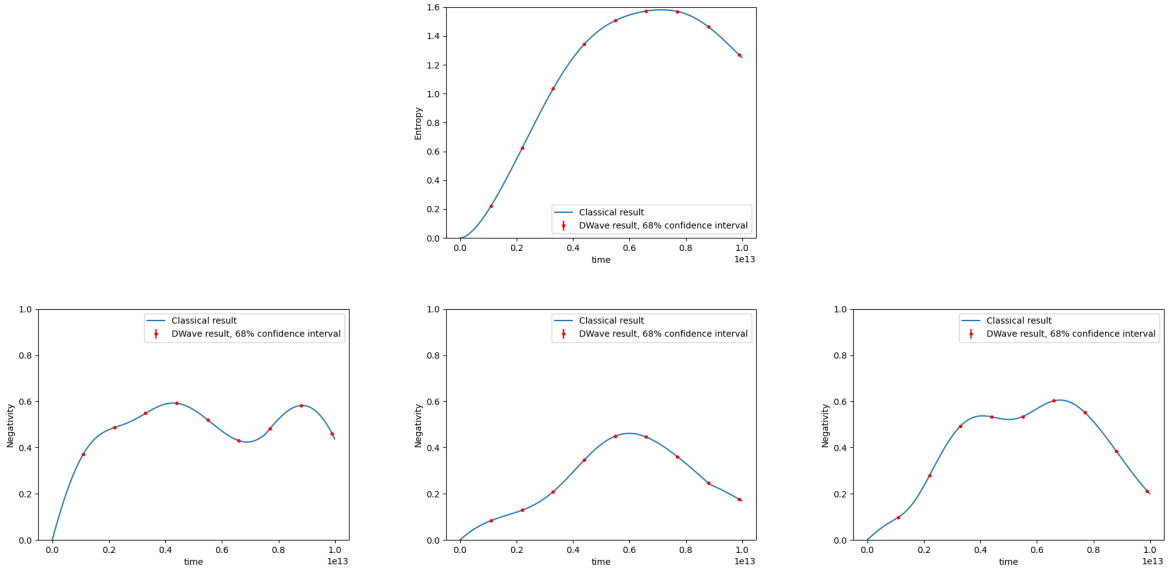


FIG. 2. A comparison of an  $N = 4$ ,  $n_f = 3$  collective neutrino oscillation results from **Advantage** and exact classical computation for entanglement entropy of the third (“probe”) neutrino (top), negativity between neutrinos 1 and 3 (bottom left), negativity between neutrinos 2 and 3 (bottom middle), and negativity between neutrinos 3 and 4 (bottom right). The initial state is  $|\nu_e\nu_e\nu_\tau\nu_\mu\rangle$  and the Hamiltonian parameters are given by Tab. I. The blue icon at the top-right indicates simulation on a quantum device [143].

## V. ATTEMPTS AT QUANTUM SCALING ADVANTAGE

The mapping of the collective neutrino oscillation system to a QUBO problem solvable on the annealer scales linearly with the size of the system’s Hilbert space. This is the same level of performance attainable with a classical device. Hence, in order to obtain a quantum advantage, a different approach is needed.

To accomplish this on **Advantage**, one must either find either a way of representing entangled states directly with the annealer’s qubits or find an observable known to be representable on the annealer’s qubits that can display the desired characteristics of the system being simulated. In the case of the latter approach, it is hypothetically possible to implement a digitization-scheme on the annealer similar to the one outlined in Section III A and have the states be mapped into a qubit basis where all of the information needed to obtain the value of the desired observable is encoded in the  $|0\rangle$  and  $|1\rangle$  states of each qubit. However, such an approach will require a discontinuous mapping to be applied to the states. Furthermore, if this kind of a feat is possible, then on gate based devices it should be possible to do most applications to physical simulations with a single shot on the device, which is far from realization. Hence, quantum scaling advantage on an annealer will most likely require putting the device’s states into a superposition of measurement-basis states. Hence, the rest of this investigation concerns methods of accomplishing this superposition.

One of the primary obstacles to quantum scaling advantage is noise. The coherence time of **Advantage**, which is  $\approx 30$  ns [144], is lower than even the lowest possible anneal-time that annealer users can access, which is 100 ns [128]. Also, in practice, **Advantage** is sufficiently noisy that the procedure in Sec. IV and App. B requires hundreds of shots and maximizing the magnitude of the parameters that fix the ground state in order to produce one shot whose result is sufficiently accurate to lead to convergence when running AQAE. With such noisy hardware, obtaining the expectation value of an observable measured on the device by averaging over multiple measurement shots, let alone state tomography, will likely be unworkable. Therefore, before quantum scaling advantage can be attempted on noisy hardware, its viability needs to be assessed for a theoretical noiseless device that anneals using the Hamiltonian given by Eq. 4.

One way to create a superposition of states is to terminate the process of annealing before it is complete. This is the most straightforward method for applications easily mappable to the quantum Ising model.

Additionally, as discussed in Section V B, measurement-based quantum computing (MBQC) can theoretically be implemented on **Advantage** this way. However, control of this process in general is highly nontrivial and requires techniques that are outside of the scope of this study. Hence, the main method for obtaining efficient scaling that I evaluated is setting  $h_i$  and  $J_{ij}$  so that multiple bitstrings have the ground-state energy, resulting in the annealer producing a frustrated state. Throughout Section V, “ $h_i$ ” and “ $J_{ij}$ ” refer to the  $h_i$  and  $J_{ij}$  terms, respectively, from Eq. 4 and “bitstring” refers to a possible state of an ideal register of qubits after a measurement in the Pauli-Z basis.

### A. Scalable qubit-mapping through frustrated states

The most basic example of a frustrated state obtainable on **Advantage** is where for a certain  $i$ ,  $h_i = 0$  and  $J_{ij} = 0$  for all  $j$ . In this case, the state of the  $i^{\text{th}}$  qubit would be  $\frac{1}{\sqrt{2}}(|\uparrow\rangle - |\downarrow\rangle)$ , because both the  $|\uparrow\rangle$  and the  $|\downarrow\rangle$  states of the  $i^{\text{th}}$  qubit have the same energy. The range of states obtainable with this method is discrete: one state per possible set of bitstrings set to the same minimal energy. In principle, it is possible to obtain a  $2^{2^{N_q}} - 1$  scaling in this way if all possible combinations of bitstrings are obtainable.

Such as scaling would be sufficient to produce quantum advantage. This is because the full state of  $N_q$  qubits on an ideal quantum device has  $2^{N_q}$  amplitudes. If these amplitudes are represented on a register of classical bits then each amplitude would need a subregister of  $K$  bits to represent, where  $K$  is a digitization-factor that works exactly the same as the one from Eq. 7. The number of states representable through this process is  $2^{K2^{N_q}}$ . Hence, I consider a representation of  $O(a^{b^{N_q}})$  discrete states with  $N_q$  qubits, where  $a$  and  $b$  are arbitrary constants, to be the benchmark for quantum scaling advantage.

One of the primary challenges facing this method is that the number of parameters submittable to Eq. 4 is  $\frac{1}{2}(N_q^2 + N_q)$  for an  $N_q$ -qubit system. Thus, if the same combinations of  $h_i$  and  $J_{ij}$  values that produce frustrated states at low  $N_q$  are the only ones that produce frustrated states as  $N_q \rightarrow \infty$ , one would get a scaling of  $O(2^{N_q^2})$  states for  $N_q$  qubits, which is insufficient to meet the quantum scaling advantage benchmark. Thus, in order to achieve the  $O(a^{b^{N_q}})$ , the number of combinations of  $h_i$  and  $J_{ij}$  that produce frustrated states would have to become denser as  $N_q$  increases. Fortunately, a cursory comparison of the  $N_q = 2$  case with larger systems suggests that frustrated state combinations do become denser as  $N_q$  increases. Specifically, with  $N_q = 2$ , there is only one  $J_{ij}$  value, so in order to generate a frustrated state, the  $J_{ij}$  value must exactly equal the impacts of the  $h_i$  values within the desired frustrated register. However, for  $N_q > 2$ , there are more  $J_{ij}$  values, and hence (in principle) more possibilities of  $J_{ij}$  values that create frustrated states.

Another challenge is that in order to create all possible energy spectra for the bitstrings obtainable on  $N_q$  qubits, one needs a Hamiltonian with all possible length- $N_q$  tensor products of one-qubit identity matrices and Pauli-Z matrices (“Pauli-Z strings”). The Hamiltonian that **Advantage** anneals to, however, only has tensor products with up to two Pauli-Z matrices. Numerous techniques for quadratization, where binary-variable functions (which sums of Pauli-Z strings are) that are of order greater than 2 are mapped onto quadratic functions have been explored in the literature surrounding quantum annealing [145–188]. However, none of these techniques are capable of quadratizing an arbitrary combination of Pauli-Z strings of length  $n$  with a better-than-exponential scaling in  $n$ . Fortunately, one does not need to create all possible energy spectra, as so long as all possible combinations of bitstrings can be set to the ground state, the non-ground-state qubits can be set to any energies above the ground state.

To evaluate the feasibility of quantum scaling advantage using the frustrated state approach, I found the number of possible combinations of bitstrings obtainable for each  $N_q$  between 1 and 4 inclusive that can share a ground state energy of  $H_f$  from Section III. Central to this process is the fact that if a set of expressions is orthogonalizable, then it is possible to make any one of them the smallest element in the set. This is because in an orthogonalizable set, it is possible to increase or decrease any element independently of the others. Additionally, I define  $n_{\text{bitstringset}}$  as the number of bitstrings set to the ground state energy of  $H_f$ .

The first step for each value of  $N_q$  is to find the highest value of  $n_{\text{bitstringset}}$  such that the set of the amplitudes of all combinations of  $n_{\text{bitstringset}}$  bitstrings is orthogonalizable. I denote this maximum value as  $n_{\text{bitstringsmax}}$ . All bitstring-combinations such that  $n_{\text{bitstringset}} \leq n_{\text{bitstringsmax}}$  are obtainable on a noiseless device that anneals to the same Hamiltonian through the correct choice of  $h_i$  and  $J_{ij}$  and hence are counted as obtainable. The solution that sets all  $h_i$  and  $J_{ij}$  to 0 is also counted.

The second step concerns  $n_{\text{bitstringsmax}} < n_{\text{bitstringset}} < 2^{N_q}$ . It is an iterative process where  $n_{\text{bitstringset}} =$

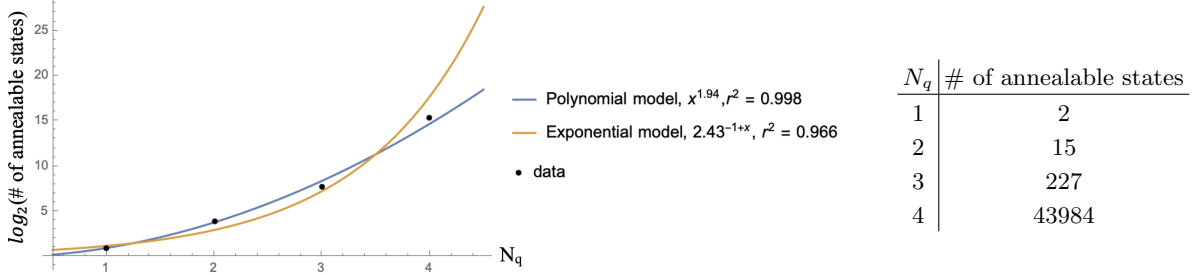


FIG. 3. On the left: polynomial and exponential fits to the base-2 logarithm of the number of annealable states of systems with various qubit-counts  $N_q$ , along with their coefficients of determination ( $r^2$ ). On the right: the numerical results for the number of annealable states for each  $N_q$ .

$2^{N_q} - 1$  for the first iteration and for each subsequent iteration is 1 less than the value for the previous iteration. During each iteration, I obtain every possible bitstring-combination that has the current iteration's value of  $n_{bitstringset}$ , and for each combination solve for the constraints on  $h_i$  and  $J_{ij}$  that would ensure that all bitstrings in the combinations have the same energy. I then delete all solutions that are either already enumerated or give the bitstrings in the solution's combination an energy of 0. All other solutions are counted as obtainable, as I have found through visual inspection that the energies that they assign all of their bitstrings form an orthonormalizable set.

After collecting the data, I took the base-2 logarithm of each number of annealable states and fitted an exponential model,  $a(b^x)$ , and a polynomial model,  $a(x^b)$ , to the results, as shown in Fig. 3. The polynomial model shows a better fit to the data, which suggests that the  $O(a^{b^{N_q}})$  benchmark is unattainable on **Advantage**, even without noise.

One final obstacle further diminishes the prospects of achieving quantum scaling advantage on **Advantage** using frustrated states. Making the energies of multiple bitstrings the same requires very precise fine-tuning of the coefficients submitted to the machine. This reduces the precision of the anneal. This was confirmed using the Julia simulated quantum annealing library QuantumAnnealing.jl. QuantumAnnealing.jl simulates the perfect anneal of the Hamiltonian in Eq. 4 on a classical device [189]. Several simulated anneals were performed for an anneal-time of 1000 ns for systems of 2 qubits, after which  $\langle \sigma^{(z)} \rangle$  is taken for the first qubit. It was found that for parameters producing states obtainable from  $|-\rangle \otimes |-\rangle$  using Clifford gates (which included the straightforwardly-obtainable bitstrings), the amplitudes were precise to 12 or more decimal places, while for other states the amplitudes were only precise to 4 decimal places. Similar results were obtained for simulations with the same anneal-time for 3-qubit systems. Such a drastic decrease in precision points to a requirement for a degree of fine-tuning that is difficult even on ideal simulations and will likely be out of reach even to the highest-fidelity near-term devices.

Thus, unless devices capable of annealing to Hamiltonians such as ZZXX and XZ [190, 191] are available, quantum annealing to a number of possible states that scales as well as the number of states encodeable on a gate-based devices will probably be out of reach.

## B. Measurement-based quantum computing

It happens that the classical Ising model Hamiltonian,  $H_f$ , that **Advantage** anneals to is the same as the Hamiltonian that can be used to obtain a cluster state for measurement-based quantum computing from the state  $|+\rangle \otimes |+\rangle \otimes \dots \otimes |+\rangle$  [192]. Since this Hamiltonian is composed of a sum of Pauli strings that are constructed entirely out of identity and  $\sigma^z$  operators, it can be adapted to do the same transformation for an initial state of  $|-\rangle \otimes |-\rangle \otimes \dots \otimes |-\rangle$  by adding a term proportional to  $\frac{\pi}{2}\sigma_i^z$  for each qubit  $i$ . Thus, one can obtain such a cluster state by starting an anneal and suddenly changing the parameters  $A(s)$  and  $B(s)$  in Eq. 4 from  $A(s) = 1, B(s) = 0$  to  $A(s) = 0, B(s) = 1$  and evolving for long enough.

An arbitrary  $SU(2)$  rotation can be written in terms of Euler angles,  $U_{rot}(\theta, \phi, \xi) = U_x(\theta)U_z(\phi)U_x(\xi)$ . It can then be implemented using measurement-based quantum computing by evolving a chain of five qubits, one with the initial state  $|\psi_i n\rangle$  and the other four in the state  $|+\rangle$  (or  $|-\rangle$ ), using the cluster-state creation Hamiltonian mentioned previously. Then, Qubits 1-4 could be measured in the basis

$$B(\phi) = \left\{ \frac{|0\rangle + e^{i\phi}|1\rangle}{\sqrt{2}}, \frac{|0\rangle - e^{i\phi}|1\rangle}{\sqrt{2}} \right\} \quad (16)$$

where  $\phi$  is 0,  $\theta$ ,  $\phi$ , and  $\xi$  for Qubits 1, 2, 3, and 4, respectively [192]. Qubit 5 would then be in the state  $U_{rot}(\theta, \phi, \xi)|\psi_i n\rangle$ , aside from some measurement-dependent corrections that can be done once the entire circuit is done and the final measurement results are obtained. The CNOT gate can be obtained in MBQC via measurements in the X and Y basis. Hence, a complete quantum computing basis can be obtained by measuring the qubits in a cluster state in basis lying on the equator of the Bloch sphere [192].

To implement this on **Advantage**, an extra rotation of  $e^{i\sigma^z\omega}$ , where  $\omega$  is the clockwise (as viewed from the +z direction) angle between the measurement axis and the positive Y-axis, would be applied to each qubit via an adjustment of the tunable Ising Hamiltonian. Then, a rotation of  $e^{i\frac{\pi}{2}\sigma^x}$  would be applied after suddenly switching the system back to  $A(s) = 1$ ,  $B(s) = 0$ .

There are several challenges to this approach as well. First, the minimum execution time for **Advantage** to execute the sudden transition, or quench, required by this process is 100 ns [128]. This imperfect sudden transition could be a source of error. The second challenge is the high level of noise and short decoherence time. Third, this method, in its present form, works by encoding the conventional gate-based quantum computing onto a quantum annealer. Thus, Trotter-error-free time evolution is generally not possible with this method, and qubit requirements are the same as an equivalent gate-based implementation times the number of time-steps in the simulation.

## VI. OTHER SYSTEMS

In the literature discussed in Section I surrounding neutrinos in the early Universe, neutron star mergers, and core-collapse supernovae, antineutrinos play an important role as neutrinos. To address the part that antineutrinos play, I discuss a method presented in Ref. [117] for adapting Eq. 1 to interactions between neutrino and antineutrino modes and produce a few of its notable results for  $n_f = 3$  in an exact classical simulation of a neutrino-antineutrino pair ( $N = 2$ ). Although recent literature utilizing mean-field theory methods have found that non-trivial effects in neutrino-antineutrino mixtures require at least  $N = 3$  [59, 193–195],  $N = 2$  is chosen as this sub-project is intended primarily as a trailhead for studies of the full  $n_f = 3$  Hilbert space. As in Section II, only coherent elastic forward scattering is taken into account.

All of the work discussed so far assumes that neutrinos are Dirac fermions. However, there are theories that stipulate that neutrinos are either Majorana fermions or have a Majorana mass [197]. Recent studies have discussed the effects of spin-flip, magnetic moment, and other non-standard neutrino interactions on Majorana neutrinos [198, 199] and have explored the possibility of using astrophysical phenomena such as white dwarfs [200] and neutron stars [201]. To see if Majorana effects are visible for entanglement observables,  $N = 2$  simulations analogous to the ones for neutrino-antineutrino pairs are done for Majorana fermions.

Finally, since collective neutrino oscillations are time-dependent in many of their physical applications, the methods and challenges in the way of implementing time-dependent collective neutrino oscillations on **Advantage** are also discussed.

### A. Neutrino-antineutrino interactions

Eq. 1 can be re-written in terms of neutrino creation and annihilation operators. The neutrino creation operator can then be set equal to the antineutrino annihilation operator and vice versa, taking advantage of CPT invariance. Besides this change, the neutrino-antineutrino interaction picks up a minus sign [39, 40, 117, 198]. This is because because the Feynman diagrams for neutrino-antineutrino interactions are odd permutations of those for neutrino-neutrino interactions [202]. The resulting additional term for neutrino-antineutrino interactions is as follows:

$$H_{\nu\bar{\nu}} = - \sum_{p,p'} k(1 - \cos\theta_{pp'}) \vec{\lambda}_p^* \cdot \vec{\lambda}_{p'} \quad (17)$$

where  $p'$  must index an antineutrino mode if  $p$  indexes a neutrino mode and must index a neutrino mode if  $p$  indexes an antineutrino mode. The superscript asterisk denotes complex conjugation. Physically, the neutrino-antineutrino interactions in Eq. 17 correspond to a weak neutral current s-channel interaction with both the initial and final state being composed of a neutrino and an antineutrino.

In principle, it is also possible for a neutrino and an antineutrino to exchange momentum through the t-channel. However, a recent study found that such interactions are helicity-suppressed. That is, they are nonexistent in the limit of massless neutrinos and in the physical reality are negligibly small given the small mass of neutrinos [196]. S-channel interactions where the modes change between neutrino and antineutrino are suppressed in the same way. Hence, Eq. 17 fully encapsulates a neutrino-antineutrino system's interactions to a very good approximation.

One marked difference between the neutrino-neutrino and neutrino-antineutrino systems is while the 2-body interaction for the former is independent of the basis that the neutrinos are in for both  $n_f=2$  and for  $n_f = 3$ , the 2-body interaction for for the former is only basis-independent for  $n_f=2$ . Hence, the full Hamiltonian for the neutrino-antineutrino term in the  $n_f=3$  case must be written with the single-neutrino terms in the flavor basis, like so:

$$H_{CNO}^{\nu\bar{\nu}} = \sum_{p=1}^N U_{PMNSp} \vec{B} \cdot \vec{\lambda}_p U_{PMNSp}^\dagger - \sum_{p,p'} k(1 - \cos \theta_{pp'}) \vec{\lambda}_p^* \cdot \vec{\lambda}_{p'} \quad (18)$$

with  $U_{PMNSp}$  and  $U_{PMNSp}^\dagger$  representing the PMNS matrix applied to the neutrino or antineutrino mode indexed by  $p$ . Additionally, the 2-body interaction does not commute with the single-neutrino oscillation term, so the reasoning behind the treatment of  $\vec{B}$  as arbitrary in Sec. IV only holds for  $n_f = 2$ . Hence, for  $n_f = 3$ ,  $\vec{B}$  is fixed to  $(0, 0, -\frac{\delta m^2}{4E}, 0, 0, 0, -\frac{\Delta m^2}{2\sqrt{3}E})$ , the value obtained in App. A.

Because the interaction term represented by Eq. 17 is not basis-independent and is specific to the flavor basis, the domain-decomposition technique used in Sec. IV to place interacting  $N = 4$  neutrino systems on **Advantage** cannot be used for neutrino-antineutrino systems. This limits the reach of quantum annealers in simulations of mixtures of neutrinos and antineutrinos.

Fig. 4 shows a comparison of results for the time evolution of entanglement entropy obtained using exact linear algebra on a classical computer for four systems with  $N = 2$  neutrinos, one for each of the following initial states:  $|\nu_e \nu_e\rangle$ ,  $|\nu_e \nu_\mu\rangle$ ,  $|\nu_e \bar{\nu}_e\rangle$ ,  $|\nu_e \bar{\nu}_\mu\rangle$ . Each two-body system is analyzed for both  $n_f = 2$  and  $n_f = 3$ . The neutrino-neutrino systems show no difference between the  $n_f = 2$  and  $n_f = 3$  results. However, for the neutrino-antineutrino systems, there is a difference. For  $n_f = 2$ , the same periodic pattern that appears in the initially  $|\nu_e \nu_\mu\rangle$  system appears in neutrino-antineutrino system, but with a lower amplitude and half the frequency. For  $n_f = 3$ , the neutrino-antineutrino entanglement entropies are more irregular. The  $|\nu_e \bar{\nu}_\mu\rangle$  system in particular shows non-periodic behavior, reminiscent of the Second Law of Thermodynamics, whereby there is a general trend towards the maximum entropy of  $\log_2(3)$ . Changing the physics to set all mixing angles to zero, or setting all mixing angles but  $\theta_{\nu 12}$  and one of the mass-difference parameters to 0, are the only ways to make it so that the  $n_f = 3$  neutrino-antineutrino result replicates the  $n_f = 2$  neutrino-antineutrino result. Physically, this suggests that another neutrino flavor inaccessible through neutrino oscillation but accessible through neutral current would be detectable through neutrino-antineutrino interactions as long as the mass of the new eigenstate does not equal the mean of the previous eigenstates' masses.

A similar analysis, shown in Fig. 5, was done for the case where only the neutrino-neutrino and neutrino-antineutrino interaction was kept, which would be a good approximation for the case immediately at the neutrinosphere, the part of the proto-neutron star from where the neutrinos stream into the outer layers from [203]. In this scenario, only initial states of  $|\nu_e \nu_\mu\rangle$  and  $|\nu_e \bar{\nu}_e\rangle$  produce entanglement. For  $n_f = 2$ , the entanglement dynamics are the same as for the neutrino-neutrino case.  $|\nu_e \bar{\nu}_e\rangle$ 's entanglement oscillations for  $n_f = 3$  have  $\frac{3}{4}$  of the frequency of, experience a bimodal character not present in, and have a higher maximum ( $\log_2(3)$  vs 1) than corresponding oscillations for  $n_f = 2$ . This  $n_f = 3$  bimodal behavior may be what manifests in more complex behavior when the single-neutrino oscillation is present. However, the nonperiodic character of the  $|\nu_e \bar{\nu}_\mu\rangle$  seems to be dependent on the existence of vacuum neutrino oscillation effects.

## B. Majorana Neutrinos

As formulated by Steven Weinberg in the 1970s, the five-dimensional Standard Model can include the following term:

$$\mathcal{L}_{Weinberg} = f_{abmn} \bar{l}_{iAL}^C l_{jBL} \phi_k^{(m)} \phi_l^{(n)} \epsilon_{ik} \epsilon_{jl} + f'_{abmn} \bar{l}_{iAL}^C l_{jBL} \phi_k^{(m)} \phi_l^{(n)} \epsilon_{ij} \epsilon_{kl} \quad (19)$$

where  $f_{abmn}$  and  $f'_{abmn}$  are coefficients with a magnitude on the order of  $\frac{1}{M}$  with  $M$  being a characteristic mass above approximately  $10^{14}$  GeV of hypothetical 'superheavy' particles,  $l_{jBL}$  is the  $j^{\text{th}}$  component of the vector in the fundamental representation of SU(2) representing a non-conserved lepton (in this case, a neutrino) with flavor  $b$  with left-handed chirality, the superscript  $C$  denotes charge-conjugation, and  $\phi_k^{(m)}$  is a scalar field that the Higgs field can be substituted in for [204]. On a staggered lattice, where each spatial lattice site  $i$  is split into two sites,  $l$  for neutrinos and  $l'$  for antineutrinos,  $\mathcal{L}_{Weinberg}$  can be converted into a Hermitian Hamiltonian form, like so:

$$H_m^{Majorana} = \frac{1}{2} m_M \sum_i (a_{il} a_{il'} + a_{il'}^\dagger a_{il}^\dagger) \quad (20)$$

with  $a$  and  $a^\dagger$  being creation and annihilation operators for the neutrino or antineutrino that exists on the staggered lattice site denoted by its subscript, with the creation operator for neutrinos being the annihilation operator for antineutrinos and vice versa. This term produces a ‘‘Majorana mass’’  $m_M$  for the neutrinos [205].

For a single-spatial-site lattice localized to spatial site  $i$ , the eigenstate of  $H_m^{Majorana}$  which has a ‘‘mass’’ of  $m_M$  is  $\frac{|\nu\rangle + |\bar{\nu}\rangle}{\sqrt{2}}$ , that is, an equal superposition of there being one neutrino on the spatial lattice site and there being one antineutrino on the spatial lattice site. This state can be interpreted as the projection of a Majorana neutrino onto the Dirac neutrino state-space used so far in this work. From this fact, one can obtain the interaction of any pair of Majorana neutrinos through direct addition of the two-neutrino term in Eq. 1 and its counterpart for antineutrino-antineutrino interactions (which is the same [117]) to the neutrino-antineutrino interaction term in Eq. 17. The resulting collective neutrino oscillation Hamiltonian for Majorana neutrinos is as follows:

$$H_{\nu\nu}^{majorana} = \sum_p U_{PMNSp} \vec{B} \cdot \vec{\lambda}_p U_{PMNSp}^\dagger + 2 * \sum_{p,p'} k(1 - \cos \theta_{pp'}) \text{Im}(\vec{\lambda}_p) \cdot \text{Im}(\vec{\lambda}_{p'}) \quad (21)$$

where  $\text{Im}()$  denotes the imaginary component. In the same manner as with the neutrino-antineutrino oscillation, the two-body interaction term is not invariant with a change of basis, so  $\vec{B}$  is fixed to the same value as in Sec. VIA.

Fig. 4 shows results for Majorana neutrinos. *A priori*, the Majorana  $|\nu_e \nu_e\rangle$  state should behave similarly to the Dirac  $|\nu_e \bar{\nu}_e\rangle$  and the Majorana  $|\nu_e \nu_\mu\rangle$  should behave similarly to the Dirac  $|\nu_e \nu_\mu\rangle$ , and several results agree with this. First, the  $n_f = 3$   $|\nu_e \nu_\mu\rangle$  initial state case shows a similar pattern of irregularity to its Dirac counterpart. Second, the Majorana  $|\nu_e \nu_e\rangle$  exhibits the same behavior as does the Dirac  $|\nu_e \bar{\nu}_e\rangle$  Third, changing the physics to set all mixing angles to zero, or to set all mixing angles but  $\theta_{\nu 12}$  and one of the mass-difference parameters to 0, are the only ways to make it so that the  $n_f = 2$  results replicate the  $n_f = 3$  results. One difference is that lower-amplitude, higher-frequency modes in the  $n_f = 3$   $|\nu_e \nu_\mu\rangle$  initial state case have a higher prominence for Majorana than for the Dirac neutrinos. Additionally, the frequency of the oscillation for periodic patterns in the Majorana is half that of counterparts in the Dirac neutrino-neutrino case. If these differences persist at asymptotically large  $N$ , neutrinos from the initial burst at the collapse of an iron core, which are probably composed primarily of electron neutrinos, could potentially be used to probe whether neutrinos are Majorana or Dirac fermions.

Similarly to Sec. VIA, the dynamics were also sampled for the case where only the collective neutrino oscillation term is included in the Hamiltonian, and the results, presented in Fig. 5, are the same as those of their Dirac counterparts. Thus, vacuum neutrino oscillation effects in dense neutrino environments are likely an explanation for the differences in the entanglement dynamics of Dirac and Majorana collective neutrino oscillations.

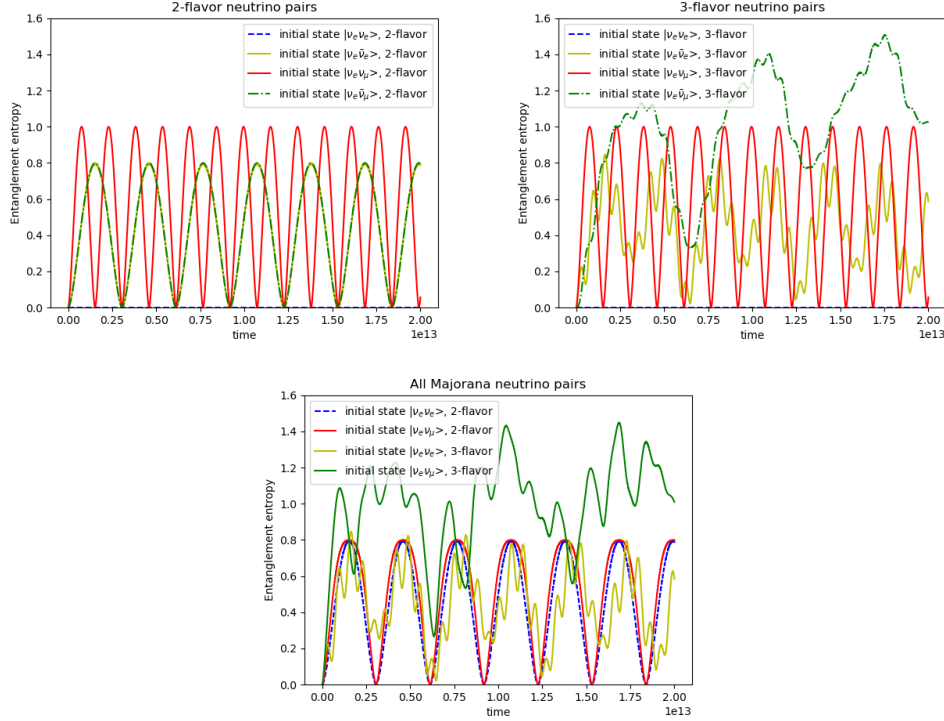


FIG. 4. Top: A comparison, which assumes the neutrinos are Dirac particles, of 2-neutrino and 1 neutrino-1 antineutrino (both  $N = 2$ ) systems' entanglement entropy evolution.  $n_f = 2$  is in the left,  $n_f = 3$  is on the right. Bottom: an analogous comparison for Majorana neutrinos. Parameters are shown in Tab. I. The purple icon at the top-right indicates exact simulation on a classical device [143].

### C. Time-dependent Hamiltonian

As mentioned at the beginning of Section II, time-dependence of neutrino-neutrino interaction, despite being physical, is excluded from this study in order to facilitate algorithm-development on the quantum annealer. With a time-independent Hamiltonian, expression of the time-evolution in the form of a QUBO matrix is a straightforward use of the time-evolution operator,  $e^{-iHt}$ . However, for a time-dependent Hamiltonian, the time-evolution operator is the time-ordered integral [202],

$$T(e^{-i \int_{t_i}^{t_f} H(t) dt}) \quad (22)$$

Thus, the use of the same techniques with a time-dependent Hamiltonian would result in an error in the calculation determined by a continuum limit of the Zassenhaus formula [206, 207],

$$e^{t(X+Y)} = e^{tX} e^{tY} e^{-\frac{t^2}{2}[X,Y]} e^{-\frac{t^3}{6}(2[Y,[X,Y]]+[X,[X,Y]])} e^{-\frac{t^4}{24}([[[X,Y],X],X]+3[[X,Y],X],Y)+3[[X,Y],Y],Y)} \dots \quad (23)$$

which removes one of the main advantages of using a quantum annealer, which is the avoidance of Trotter errors. It is possible to avoid these Trotter errors, but that would require the Schrödinger equation to be fully solved in order to represent the time evolution in QUBO form, which is sufficient to find the time evolution by itself.

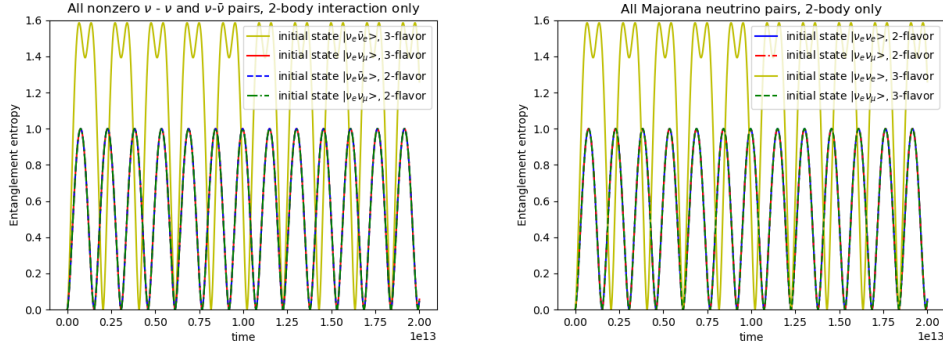


FIG. 5. A comparison of Dirac and Majorana  $N = 2$  neutrino systems' entanglement entropy evolution for  $n_f = 2$  and  $n_f = 3$ , representative of all scenarios that produce nonzero results. Parameters are the same as those in Tab. I. The purple icon at the top-right indicates exact simulation on a classical device [143].

## VII. CONCLUSION

This work has presented the time-evolution of the entanglement structure of multi-angle, three-flavor coherent collective neutrino oscillations on a quantum annealer. Successful verification of annealer results and extension to neutrino-antineutrino and Majorana neutrino pair dynamics using exact numerical calculations have also been discussed. Following the direction of Ref. [81], the Feynman Clock method was used to encode the coherent collective neutrino oscillation dynamics onto a Hamiltonian whose ground state emulates the desired time-evolution. The Adaptive Quantum Annealing Eigensolver (AQAE) method was then used to obtain said ground state. Fitting  $N = 4$  neutrinos that each have  $n_f = 3$  possible flavors onto the limited number of logical qubits available required the use of domain-decomposition. This was accomplished by taking advantage of the fact that in the mass-basis, the collective neutrino oscillation Hamiltonian is naturally block-diagonalized. This technique is only possible with a neutrino-neutrino interaction that is invariant with respect to neutrino-basis transformation under the Pontecorvo–Maki–Nakagawa–Sakata (PMNS) matrix. Therefore, while it works for systems of Dirac neutrinos, it does not work for neutrino-antineutrino mixtures or for Majorana neutrinos.

AQAE can reproduce collective neutrino oscillation dynamics without Trotter errors for  $n_f = 3$ , just like how it was able to for  $n_f = 2$  in Ref. [81], and do so with a precision equal to the maximum attainable with the double-precision floating point format on classical computers. However, its qubit-requirements do not scale any better than do those of classical devices. Direct encoding of a scalable number of states on an annealer utilizing the Hamiltonian in Eq. 4 using frustrated states is hindered by margins for error that are difficult to satisfy even on ideal emulators and the fact that the number of states annealable-to using this method probably scales exponentially worse than what is required for a quantum advantage. Thus, it will likely take annealers with alternative choices of  $H_\alpha$  (in Section III's parlance), such as the ZZXX and the ZX Hamiltonian [190, 191], for quantum annealing to see the scaling advantage of conventional gate-based qubit devices. It is theoretically possible to obtain an exponential improvement in scaling on **Advantage**, by utilizing its  $H_\alpha$  to implement measurement-based quantum computing. However, this approach does not eliminate Trotter errors and will likely struggle with the fact that the decoherence time of **Advantage** ( $\approx 30$  ns) is shorter than any anneal-time available on the device ( $\geq 100$  ns) and with errors from the non-instantaneous quenches that the device is limited to. This is in addition to the sources of noise that existing annealing algorithms already have to contend with.

D-Wave Inc.'s new **Advantage2** annealer has more qubits, longer coherence time ( $\approx 300$  ns compared to **Advantage**'s  $\approx 30$  ns), and less noise than **Advantage** [208]. Thus, it is possible that paths toward quantum advantage on annealers could be explored on **Advantage2** and its successors. However, the best qubit-scaling that I found to be theoretically possible with current methods of modeling time-evolution on D-Wave Inc.'s annealers is that of the equivalent gate-based implementation times the number of time-steps in the simulation. Given this finding, combined with the fact that gate-based devices with thousands of qubits, such



as such as IBM’s Condor processor, exist and are expected to grow in capability [209], gate-based devices look to be more promising than annealers for realizing quantum advantage for time-evolution simulations. Quantum annealers will most likely be more suited towards optimization problems, as recent studies have found evidence that quantum annealing and classical simulation of quantum annealing achieve equal to superior performance over conventional classical algorithms [210–213] and gate-based quantum approaches [214] for several optimization problems.

For the case of a pure Dirac neutrino sample without antineutrinos, I have found that the entanglement dynamics of neutrinos with the physical  $n_f = 3$  are different from what can be produced by an  $n_f = 2$  system if and only if all three neutrino flavors are present in the initial state. This suggests that for a near purely  $\nu_e$  sample, which is likely a close approximation of the composition of the neutrinos first emitted as the iron core of a massive star collapses [24–26], relevant three-flavor dynamics can be simulated efficiently on classical computers with methods such as mean field theory, while any entangling phenomena can be obtained using a two-flavor simulation. This is in contrast to results from Ref. [72], which showed a difference in results between two-flavor and three-flavor models for a system whose initial state is entirely composed of electron neutrinos. One possible explanation for this apparent discrepancy is that a difference between  $n_f = 2$  and  $n_f = 3$  manifests itself when either the neutrino-neutrino interaction is time-dependent or the neutrino modes have different energies, and investigation of this is a potential topic for future work.

However, if physical neutrinos are Majorana fermions, the findings of this work suggest a far different outcome. Even for the simple case where the number of neutrinos,  $N$ , is 2, Majorana neutrino entanglement shows a marked difference in behavior between  $n_f = 2$  and  $n_f = 3$  for all initial states. This result indicates that the entanglement structure of the initial burst of electron neutrinos from the core-collapse of a massive star can potentially indicate if neutrinos exhibit a Majorana mass or not. Thus, the behavior of collective Majorana neutrino oscillations in larger systems and their effects on supernova observables are a potential next step. It is important to note that the divergent behavior of Majorana fermions observed in this study is dependent on both vacuum neutrino oscillation and neutrino-neutrino interactions having a non-negligible effect, so the best place to look for this behavior is likely the transition region between the interaction-dominated regime and the vacuum oscillation-dominated regime.

O(1 second) after core collapse, the neutrinos from the core are expected to be a roughly even mixture of all three flavors and of neutrinos and antineutrinos [24–26]. For such a system, I have found that  $n_f = 3$  entanglement dynamics are distinct from those for  $n_f = 2$ . This is due to two reasons. The first is the difference with  $n_f = 2$  behavior exhibited by a state that starts as a mixture of all three flavors. The second is because, similar to Majorana neutrinos, neutrino-antineutrino mixtures show substantial differences between  $n_f = 2$  and  $n_f = 3$  even for the simple  $N = 2$  case when both neutrino-neutrino interactions and vacuum oscillations have non-negligible effects on flavor dynamics. In conclusion, a simulation of larger- $N$  neutrino-antineutrino mixtures with all three flavors equally represented could be an ideal substrate for realizing quantum advantage.

This study is intended primarily as a demonstration, so there are several directions in which future work could proceed, besides the straightforward expansion of  $n_f = 3$  dynamics to larger-capacity quantum devices. The first is to evaluate the full neutral current neutrino-neutrino interaction and compare its entanglement dynamics to that found in the coherent forward scattering approximation. The second is to find a method of evaluating neutrino-antineutrino interactions either on quantum annealers or on gate-based devices and to do so for at least three modes (which Refs. [215–218] found to be the minimum  $N$ -value for which mean-field instabilities occur). This could be a first step towards realizing quantum advantage in  $n_f = 3$  environments with an even mixture of neutrinos and antineutrinos of all 3 flavors. Third, until quantum computers sufficiently large-scale and high-fidelity to simulate collective neutrino dynamics at a macroscopic scale become available, methods of modifying mean-field theory to successfully model  $n_f = 3$  quantum entanglement effects on astrophysical observables, along with other macroscopic heuristics, will be important to develop. A fourth direction is repeating for  $n_f = 3$  searches for conserved quantities, Loschmidt echoes, thermalization, dynamical phase transitions, and other phenomena that have been conducted for  $n_f = 2$  [45–51, 53–55, 57, 58, 61, 62].

## ACKNOWLEDGEMENTS

This work was supported in part by U.S. Department of Energy, Office of Science, Office of Nuclear Physics, InQubator for Quantum Simulation (IQuS) [219] under Award Number DOE (NP) Award DE-

SC0020970 via the program on Quantum Horizons: QIS Research and Innovation for Nuclear Science and by the Quantum Computing Summer School 2023 at Los Alamos National Laboratory (LANL) [220].

I acknowledge the use of DWave Systems Inc.'s services for this work [221]. The views expressed are those of the author and do not reflect the official policy or position of DWave Systems. In this paper, I used **Advantage**, DWave Systems's latest device as of the beginning of this project. This project also made extensive use of Python, Wolfram Mathematica, and Julia. Two of the most important libraries used were DWave Systems's Ocean environment and the QuantumAnnealing Julia library, developed by Carleton Coffrin and Zachary Morrell [222].

I would like to thank Carleton Coffrin and Zachary Morrell from LANL for guiding me through the use of DWave's systems and assisting with access to DWave's machines. I would also like to thank Professor Martin Savage at IQuS and Joseph Carlson at LANL's T-2 group for their mentorship throughout this project, for creating the idea of a neutrino project on D-Wave Inc.'s devices, and for helping secure access to the **Advantage** annealer. Additionally, I would like to thank the staff involved in the organization of the Quantum Computing Summer School (QCSS) at LANL, particularly Lukasz Cincio and Marco Cerezo. I would also like to thank my colleagues from iQuS, Stephan Caspar, Francesco Turro, and Marc Illa, for valuable discussions. Finally, I would like to thank my colleagues from the T-2 group, Joshua Martin, Ionel Stetcu, and Ronen Weiss, both for valuable discussions and for assistance with access to DWave Systems Inc.'s software and devices.

### Appendix A: Derivation of the $n_f = 3$ single-neutrino oscillation Hamiltonian term

First, assuming that the velocity, and hence the momentum of all 3 mass-eigenstates of the neutrino are the same, and expressing each eigenstate's energy using the relativistic energy formula, the Hamiltonian is as follows:

$$H_\nu = \sqrt{m_1^2 + p^2} |1\rangle \langle 1| + \sqrt{m_2^2 + p^2} |2\rangle \langle 2| + \sqrt{m_3^2 + p^2} |3\rangle \langle 3| \quad (\text{A1})$$

In the ultrarelativistic limit, which neutrinos with energies of 10 MeV can be approximated to be in, one can take the Taylor expansion of the square root function around the zero-mass limit:

$$H_\nu = p \left(1 + \frac{m_1^2}{2p^2}\right) |1\rangle \langle 1| + p \left(1 + \frac{m_2^2}{2p^2}\right) |2\rangle \langle 2| + p \left(1 + \frac{m_3^2}{2p^2}\right) |3\rangle \langle 3| \quad (\text{A2})$$

Because the zero-point of energy is arbitrary, one can simply subtract the identity matrix times  $(p + \frac{m_1^2 + m_2^2 + m_3^2}{6p^2})$  to make the Hamiltonian traceless:

$$H_\nu = \frac{2m_1^2 - m_2^2 - m_3^2}{6p} |1\rangle \langle 1| + \frac{2m_2^2 - m_1^2 - m_3^2}{6p} |2\rangle \langle 2| + \frac{2m_3^2 - m_1^2 - m_2^2}{6p} |3\rangle \langle 3| \quad (\text{A3})$$

Defining  $\delta m^2 = m_2^2 - m_1^2$  and  $\Delta m^2 = m_3^2 - \frac{m_2^2 + m_1^2}{2}$ , one can get

$$H_\nu = \frac{-\frac{3}{2}\delta m^2 - \Delta m^2}{6p} |1\rangle \langle 1| + \frac{\frac{3}{2}\delta m^2 - \Delta m^2}{6p} |2\rangle \langle 2| + \frac{\Delta m^2}{3p} |3\rangle \langle 3| \quad (\text{A4})$$

And given that in the ultrarelativistic limit,  $p \simeq E$ ,

$$H_\nu = \left(-\frac{\delta m^2}{4E} - \frac{\Delta m^2}{6E}\right) |1\rangle \langle 1| + \left(\frac{\delta m^2}{4E} - \frac{\Delta m^2}{6E}\right) |2\rangle \langle 2| + \left(\frac{\Delta m^2}{3E}\right) |3\rangle \langle 3| \quad (\text{A5})$$

Or:

$$H_\nu = -\frac{\delta m^2}{4E} \lambda_3 - \frac{\Delta m^2}{2\sqrt{3}E} \lambda_8 \quad (\text{A6})$$

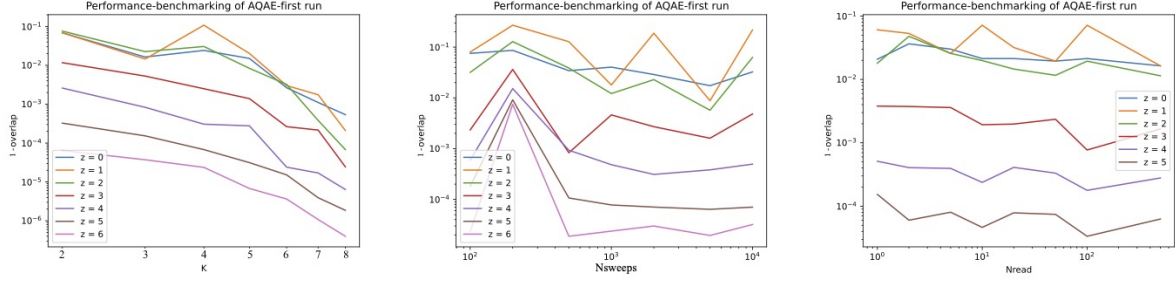


FIG. 6. From left to right, the effect of  $z$  and  $K$ , of  $z$  and the number of sweeps in an anneal (which is a surrogate for anneal-time), and of  $z$  and the number of anneal-repetitions per call to the annealer on  $1$  minus the dot product of the final state-vector of the time-evolution of 2 neutrinos as calculated by Neal and the same state-vector as calculated using exact linear algebra. The initial state is  $|\nu_e\nu_\mu\rangle$ , the Hamiltonian used for the evolution is Equation 1, the parameters are found in Table I, and the time-interval evolved over is  $10^{12} eV^{-1}$ . Each entry is the lowest-energy final result out of all the anneal-repetitions in its AQAE step. The yellow icon at the top-right indicates a noisy classical simulation [143].

## Appendix B: Benchmarking

AQAE's performance depends on the number of repetitions of the anneal, the annealing time, and the constants  $K$  and  $z$  in Eq. 10 and 12 which determine the digitization and the number of zoom-steps. Thus, the first step before running any process on the annealer is to use D-Wave's simulated classical thermal annealer, `neal`, to assess the best way to use these parameters to optimize device performance. The Hamiltonian in Eq. 1 was used in this case, with  $N = 2$ . The parameters are the same ones in Tab. I.  $\vec{B}$  was simply taken from Ref. [72]:  $\vec{B} = (0, 0, -\frac{\delta m^2}{4E}, 0, 0, 0, -\frac{\Delta m^2}{4E})$ . The starting state was  $|\nu_e\nu_\mu\rangle$ . The time-increment evolved over was  $t = 10^{12} eV^{-1}$ . The reverse-digitization process and the fixing of the penalty term  $h_i$  values discussed in Section III were not used; instead, the digitization procedure and the penalty term were found in the same manner as in Ref. [81]. In doing so, I replicate Ref. [81]'s result that increasing  $z$  produces a much greater improvement in precision than any of the above options, as seen in Fig. 6.

Thus,  $K$ , anneal-time, and the number of repetitions of each anneal-step only need to be adequate to converge, and once that is assured, the way to improve precision is to increase  $z$ . The next step is to assess how many zoom-steps are needed in order to converge to a satisfactory precision. This was done by running the same simulation on `Advantage`, with the reverse-digitization and fixing of the penalty term  $h_i$  values included. Annealer parameters were  $K = 2$ , anneal-time  $5 \mu s$ , 1000 repetitions of each zoom-step, and a chain-strength of 1. As seen in Fig. 7, it takes about 26 zoom-steps to converge.

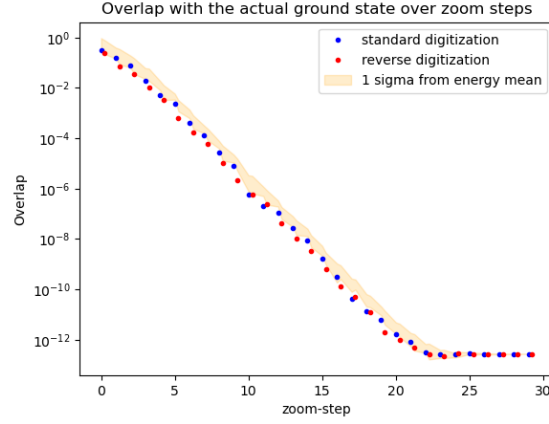


FIG. 7. The overlap between results of time-evolution with AQAE of a three-flavor, two-neutrino system starting as one electron and one muon neutrino and evolved over a time-increment of  $10^{10}eV^{-1}$  and the actual final state.  $N_{reads} = 1000$ ,  $a_t = 20 \mu s$ ,  $K = 1$ , and chain-strength = 1. The blue icon at the top-right indicates simulation on a quantum device [143].

### Appendix C: Tables of $N = 4$ $\nu$ - $\nu$ results for entanglement witnesses

time ( $eV^{-1}$ )	$S_3(t)$
$1.1 * 10^{12}$	$0.222927229(^{+619}_{-1527})$
$2.2 * 10^{12}$	$0.623264640(^{+50}_{-3222})$
$3.3 * 10^{12}$	$1.0340534849(^{+1546}_{-660})$
$4.4 * 10^{12}$	$1.3420253885(^{+18009}_{-6643})$
$5.5 * 10^{12}$	$1.5060393872(^{+2875}_{-67})$
$6.6 * 10^{12}$	$1.5718841229(^{+252}_{-308})$
$7.7 * 10^{12}$	$1.5693430609(^{+6021}_{-1011})$
$8.8 * 10^{12}$	$1.4631204675(^{+109}_{-6577})$
$9.9 * 10^{12}$	$1.2671452598(^{+451}_{-54})$

TABLE II. A table of the D-Wave **Advantage** quantum annealer results for entanglement entropy for the third neutrino of the  $N = 4$ ,  $n_f = 3$  system results from Fig. 2. Error bars are  $1\sigma$  confidence intervals.

time ( $eV^{-1}$ )	$N_{13}(t)$	$N_{23}(t)$	$N_{34}(t)$
$1.1 * 10^{12}$	$0.3720986223^{(+10285, -17470)}$	$0.0842779937^{(+2064, -9353)}$	$0.0984672558^{(+4280, -16009)}$
$2.2 * 10^{12}$	$0.4868408929^{(+104, -13601)}$	$0.1291148436^{(+194, -692)}$	$0.2787261578^{(+144, -4655)}$
$3.3 * 10^{12}$	$0.5484990103^{(+712, -7655)}$	$0.2091610157^{(+20706, -110)}$	$0.4936497469^{(+94, -18696)}$
$4.4 * 10^{12}$	$0.5918213991^{(+694, -5279)}$	$0.3460545631^{(+2102, -12006)}$	$0.5329880752^{(+7887, -255)}$
$5.5 * 10^{12}$	$0.5197404555^{(+117, -1131)}$	$0.4497961383^{(+364, -654)}$	$0.5347131445^{(+495, -387)}$
$6.6 * 10^{12}$	$0.4301304886^{(+1428, -64)}$	$0.4458340852^{(+35, -3029)}$	$0.6025444696^{(+695, -33)}$
$7.7 * 10^{12}$	$0.4824124333^{(+18476, -461)}$	$0.3611637035^{(+388, -22517)}$	$0.5514675837^{(+731, -19224)}$
$8.8 * 10^{12}$	$0.5822152101^{(+371, -1104)}$	$0.2461251687^{(+351, -5615)}$	$0.3860333315^{(+438, -1888)}$
$9.9 * 10^{12}$	$0.4597905236^{(+16, -956)}$	$0.1754865412^{(+301, -18)}$	$0.2120581628^{(+1237, -18)}$

TABLE III. A table of the D-Wave **Advantage** quantum annealer results for negativities for the third neutrino of the  $N = 4$ ,  $n_f = 3$  system results from Fig. 2. Error bars are  $1\sigma$  confidence intervals.

- 
- [1] H.-T. Janka, K. Langanke, A. Marek, G. Martínez-Pinedo, and B. Müller, Theory of core-collapse supernovae, *Progress in Particle and Nuclear Physics* **57**, 142 (2007).
  - [2] A. Mezzacappa, Toward realistic models of core collapse supernovae: A brief review, in *Proceedings of the International Astronomical Union, Symposium S362: The Predictive Power of Computational Astrophysics as a Discovery Tool*, Vol. 16 (2020) pp. 215–227.
  - [3] A. Burrows and D. Vartanyan, Core-collapse supernova explosion theory, *Nature* **589**, 29 (2021).
  - [4] G. M. Fuller and W. C. Haxton, Neutrinos in Stellar Astrophysics, in *The Encyclopedia of Cosmology* (World Scientific Series in Astrophysics, 2023) pp. 367–431.
  - [5] F. Foucart, Neutrino transport in general relativistic neutron star merger simulations, *Living Reviews in Computational Astrophysics* **9**, 1 (2023).
  - [6] M. Ruffert, H.-T. Janka, K. Takahashi, and G. Schäfer, Coalescing neutron stars – a step towards physical models II. Neutrino emission, neutron tori, and gamma-ray bursts, *Astronomy & Astrophysics* **319**, 122 (1997).
  - [7] D. Radice, A. Perego, S. Bernuzzi, and B. Zhang, Long-lived remnants from binary neutron star mergers, *Monthly Notices of the Royal Astronomical Society* **481**, 3670 (2018).
  - [8] V. Nedora *et al.*, Numerical Relativity Simulations of the Neutron Star Merger GW170817: Long-term Remnant Evolutions, Winds, Remnant Disks, and Nucleosynthesis, *The Astrophysical Journal* **906**, 98 (2021), 20pp.
  - [9] R. Bowers and J. R. Wilson, Collapse of Iron Stellar Cores, *The Astrophysical Journal* **263**, 366 (1982).
  - [10] S. E. Woosley, P. A. Pinto, and L. Ensman, Supernova 1987a-Six weeks later, *The Astrophysical Journal* **324**, 466 (1988).
  - [11] M. Turatto *et al.*, The Peculiar Type II Supernova 1997D: A Case for a Very Low  $^{56}\text{Ni}$  Mass, *The Astrophysical Journal* **498**, L129 (1998).
  - [12] J. Sollerman, R. J. Cumming, and P. Lundqvist, A Very Low Mass of  $^{56}\text{Ni}$  in the Ejecta of SN 1994WA, *The Astrophysical Journal* **493**, 933 (1998).
  - [13] M. Nicholl *et al.*, An extremely energetic supernova from a very massive star in a dense medium, *Nature Astronomy* **4**, 893 (2020).
  - [14] N. Smith *et al.*, SN 2006gy: Discovery of the most luminous supernova ever recorded, powered by the death of an extremely massive star like  $\eta$  Carinae, *The Astrophysical Journal* **666**, 1116 (2007).
  - [15] A. J. Drake, S. G. Djorgovski, J. L. Prieto, A. Mahabal, D. Balam, R. Williams, M. J. Graham, M. Catelan, E. Beshore, and S. Larson, Discovery of the extremely energetic supernova 2008fz, *The Astrophysical Journal Letters* **718**, L127 (2010).
  - [16] E. Chatzopoulos, J. C. Wheeler, J. Vinko, R. Quimby, E. L. Robinson, A. A. Miller, R. J. Foley, D. A. Perley, F. Yuan, C. Akerlof, and J. S. Bloom, SN 2008am: A super-luminous Type II<sub>n</sub> supernova, *The Astrophysical Journal* **729**, 143 (2011).
  - [17] A. Rest *et al.*, Pushing the boundaries of conventional core-collapse supernovae: The extremely energetic supernova SN 2003ma, *The Astrophysical Journal* **729**, 88 (2011).
  - [18] S. Benetti *et al.*, The supernova CSS121015:004244+132827: a clue for understanding superluminous supernovae, *Monthly Notices of the Royal Astronomical Society* **472**, 1538 (2017).
  - [19] G. Pagliaroli, F. Vissani, M. L. Costantini, and A. Ianni, Improved analysis of SN1987a antineutrino events, *Astroparticle Physics* **31**, 163 (2009).
  - [20] S. A. Colgate and R. H. White, The Hydrodynamic Behavior of Supernovae Explosions, *Astrophysical Journal* **143**, 626 (1966).

- [21] W. Arnett, Gravitational collapse and weak interactions, *Canadian Journal of Physics* **44**, 2553 (1966).
- [22] J. R. Wilson, Supernovae and Post-Collapse behavior, in *Numerical Astrophysics*, edited by J. Centrella, J. M. LeBlanc, and R. Bowers (1985) p. 422.
- [23] H. A. Bethe and J. R. Wilson, Revival of a stalled supernova shock by neutrino heating, *The Astrophysical Journal* **295**, 14 (1985).
- [24] T. Fischer, G. Martínez-Pinedo, M. Hempel, and M. Liebendörfer, Neutrino spectra evolution during protoneutron star deleptonization, *Phys. Rev. D* **85**, 083003 (2012).
- [25] T. Fischer, S. C. Whitehouse, A. Mezzacappa, F.-K. Thielemann, and M. Liebendörfer, Protoneutron star evolution and the neutrino-driven wind in general relativistic neutrino radiation hydrodynamics simulations, *A&A* **517**, A80 (2010).
- [26] L. Hüdepohl, B. Müller, H.-T. Janka, A. Marek, and G. G. Raffelt, Neutrino Signal of Electron-Capture Supernovae from Core Collapse to Cooling, *PRL* **104**, 251101 (2010).
- [27] M. J. Savage, R. A. Malaney, and G. M. Fuller, Neutrino oscillations and the leptonic charge of the universe, *The Astrophysical Journal* **368**, 1 (1991).
- [28] Y.-Z. Qian, G. M. Fuller, G. J. Mathews, R. W. Mayle, J. R. Wilson, and S. E. Woosley, Connection between Flavor Mixing of Cosmologically Significant Neutrinos and Heavy Element Nucleosynthesis in Supernovae, *Physical Review Letters* **71**, 1977 (1993).
- [29] C. Fröhlich, G. Martínez-Pinedo, M. Liebendörfer, F.-K. Thielemann, E. Bravo, W. Hix, K. Langanke, and N. Zinner, Neutrino-Induced Nucleosynthesis of  $A > 64$  Nuclei: The  $\nu p$  Process, *Physical Review Letters* **96**, 142502 (2006).
- [30] E. Grohs and G. M. Fuller, The surprising influence of late charged current weak interactions on Big Bang Nucleosynthesis, *Nuclear Physics B* **911**, 955 (2016).
- [31] O. Just, A. Bauswein, R. Ardevol Pulpillo, S. Goriely, and H.-T. Janka, Comprehensive nucleosynthesis analysis for ejecta of compact binary mergers, *MNRAS* **448**, 541 (2015).
- [32] S. Wanajo, The rp-process in neutrino-driven winds, *The Astrophysical Journal* **647**, 1323 (2006).
- [33] S. Woosley, D. Hartmann, R. Hoffman, and W. Haxton, The  $\nu$ -process, *Astrophysical Journal*, Part 1 (ISSN 0004-637X), vol. 356, June 10, 1990, p. 272-301. Research supported by the Los Alamos National Laboratory and University of California. **356**, 272 (1990).
- [34] L. Roberts, S. Woosley, and R. Hoffman, Integrated nucleosynthesis in neutrino-driven winds, *The Astrophysical Journal* **722**, 954 (2010).
- [35] H. Sasaki, T. Kajino, T. Takiwaki, T. Hayakawa, A. Balantekin, and Y. Pehlivan, Possible effects of collective neutrino oscillations in three-flavor multiangle simulations of supernova  $\nu p$  processes, *Physical Review D* **96**, 043013 (2017).
- [36] A. Balantekin, M. J. Cervia, A. V. Patwardhan, R. Surman, and X. Wang, Collective neutrino oscillations and heavy-element nucleosynthesis in supernovae: exploring potential effects of many-body neutrino correlations, *arXiv preprint arXiv:2311.02562* (2023).
- [37] H. Duan, The influence of collective neutrino oscillations on a supernova r process, *Journal of Physics G: Nuclear and Particle Physics* **38**, 035201 (2011).
- [38] G. M. Fuller, R. W. Mayle, J. R. Wilson, and D. N. Schramm, Resonant Neutrino Oscillations and Stellar Collapse, *The Astrophysical Journal* **322**, 795 (1987).
- [39] D. Nötzold and G. Raffelt, Neutrino dispersion at finite temperature and density, *Nuclear Physics B* **307**, 924 (1988).
- [40] G. Sigl and G. Raffelt, General kinetic description of relativistic mixed neutrinos, *Nuclear Physics B* **406**, 423 (1993).
- [41] Y.-Z. Qian and G. M. Fuller, Neutrino-neutrino scattering and matter-enhanced neutrino flavor transformation in supernovae, *Physical Review D* **51**, 1479 (1995).
- [42] S. Shalgar and I. Tamborra, Do we have enough evidence to invalidate the mean-field approximation adopted to model collective neutrino oscillations?, *Physical Review D* **107**, 123004 (2023).
- [43] H. Bethe, Zur Theorie der Metalle, *Zeitschrift für Physik* **71**, 205 (1931).
- [44] G. Vidal, Efficient Classical Simulation of Slightly Entangled Quantum Computations, *Physical Review Letters* **91**, 147902 (2003).
- [45] Y. Pehlivan, A. B. Balantekin, T. Kajino, and T. Yoshida, Invariants of collective neutrino oscillations, *Physical Review D* **84**, 065008 (2011).
- [46] C. Espinoza, C. Volpe, and D. Vaeaenaenen, Extended evolution equations for neutrino propagation in astrophysical and cosmological environments, *Physical Review D* **87**, 113010 (2013).
- [47] Y. Pehlivan, A. B. Balantekin, and T. Kajino, Neutrino magnetic moment, CP violation, and flavor oscillations in matter, *Physical Review D* **90**, 065011 (2014).
- [48] S. Birol, Y. Pehlivan, A. B. Balantekin, and T. Kajino, Neutrino spectral split in the exact many-body formalism, *Physical Review D* **98**, 083002 (2018).
- [49] M. J. Cervia, A. V. Patwardhan, and A. B. Balantekin, Symmetries of Hamiltonians describing systems with arbitrary spins, *International Journal of Modern Physics E* **28**, 1950032 (2019).

- [50] M. J. Cervia, A. V. Patwardhan, A. B. Balantekin, S. N. Coppersmith, and C. W. Johnson, Entanglement and collective flavor oscillations in a dense neutrino gas, *Phys. Rev. D* **100**, 083001 (2019).
- [51] A. V. Patwardhan, M. J. Cervia, and A. B. Balantekin, Eigenvalues and eigenstates of the many-body collective neutrino oscillation problem, *Physical Review D* **99**, 123013 (2019).
- [52] E. Rrapaj, Exact solution of multiangle quantum many-body collective neutrino-flavor oscillations, *Physical Review C* **101**, 065805 (2020).
- [53] A. V. Patwardhan, M. J. Cervia, and A. B. Balantekin, Spectral splits and entanglement entropy in collective neutrino oscillations, *Physical Review D* **104**, 123035 (2021).
- [54] A. Roggero, Dynamical phase transitions in models of collective neutrino oscillations, *Physical Review D* **104**, 123023 (2021).
- [55] A. Roggero, Entanglement and many-body effects in collective neutrino oscillations, *Physical Review D* **104**, 103016 (2021).
- [56] M. J. Cervia, P. Siwach, A. V. Patwardhan, A. B. Balantekin, S. N. Coppersmith, and C. W. Johnson, Collective neutrino oscillations with tensor networks using a time-dependent variational principle, *Physical Review D* **105**, 123025 (2022).
- [57] D. Lacroix, A. B. Balantekin, M. J. Cervia, A. V. Patwardhan, and P. Siwach, Role of non-Gaussian quantum fluctuations in neutrino entanglement, *Physical Review D* **106**, 123006 (2022).
- [58] J. D. Martin, A. Roggero, H. Duan, and J. Carlson, Many-body neutrino flavor entanglement in a simple dynamic model, (2023), arXiv:2301.07049 [hep-ph].
- [59] D. F. G. Fiorillo and G. G. Raffelt, Slow and fast collective neutrino oscillations: Invariants and reciprocity, *Physical Review D* **107**, 043024 (2023).
- [60] J. D. Martin, D. Neill, A. Roggero, H. Duan, and J. Carlson, Equilibration of quantum many-body fast neutrino flavor oscillations, *Physical Review D* **108**, 123010 (2023).
- [61] V. Cirigliano, S. Sen, and Y. Yamauchi, Neutrino many-body flavor evolution: the full Hamiltonian, arXiv preprint arXiv:2404.16690 (2024).
- [62] R. Bhaskar, A. Roggero, and M. J. Savage, Time Scales in Many-Body Fast Neutrino Flavor Conversion, (2024), arXiv:2312.16212v2 [nucl-th].
- [63] D. Neill, H. Liu, J. Martin, and A. Roggero, Scattering neutrinos, spin models, and permutations, arXiv preprint arXiv:2406.18677 (2024).
- [64] A. Friedland and C. Lunardini, Do many-particle neutrino interactions cause a novel coherent effect?, *Journal of High Energy Physics* **2003**, 043 (2003).
- [65] A. Friedland, B. H. J. McKellar, and I. Okuniewicz, Construction and analysis of a simplified many-body neutrino model, *Physical Review D* **73**, 093002 (2006).
- [66] Z. Xiong, Many-body effects of collective neutrino oscillations, *Physical Review D* **105**, 103002 (2022).
- [67] A. Roggero, E. Rrapaj, and Z. Xiong, Entanglement and correlations in fast collective neutrino flavor oscillations, *Physical Review D* **106**, 043022 (2022).
- [68] J. D. Martin, A. Roggero, H. Duan, J. Carlson, and V. Cirigliano, Classical and quantum evolution in a simple coherent neutrino problem, *Physical Review D* **105**, 083020 (2022).
- [69] A. Balantekin, M. J. Cervia, A. V. Patwardhan, E. Rrapaj, and P. Siwach, Quantum information and quantum simulation of neutrino physics, *Eur. Phys. J. A* **59**, 186 (2023).
- [70] B. Hall, A. Roggero, A. Baroni, and J. Carlson, Simulation of collective neutrino oscillations on a quantum computer, *Physical Review D* **104**, 063009 (2021).
- [71] A. Patwardhan, M. Cervia, E. Rrapaj, P. Siwach, and A. Balantekin, Many-Body Collective Neutrino Oscillations: Recent Developments, in *Handbook of Nuclear Physics*, edited by I. Tanihata, H. Toki, and T. Kajino (Springer, Singapore, 2023).
- [72] P. Siwach, A. M. Suliga, and A. B. Balantekin, Entanglement in three-flavor collective neutrino oscillations, *Physical Review D* **107**, 10.1103/PhysRevD.107.023019 (2023).
- [73] U. Schollwöck, The density-matrix renormalization group in the age of matrix product states, *Annals of physics* **326**, 96 (2011).
- [74] S. Paeckel, T. Köhler, A. Swoboda, S. R. Manmana, U. Schollwöck, and C. Hubig, Time-evolution methods for matrix-product states, *Annals of Physics* **411**, 167998 (2019).
- [75] R. P. Feynman, Simulating physics with computers, *International Journal of Theoretical Physics* **21**, 467 (1982).
- [76] S. Lloyd, Universal Quantum Simulators, *Science* **273**, 1073 (1996).
- [77] M. Ila and M. J. Savage, Multi-Neutrino Entanglement and Correlations in Dense Neutrino Systems, *Physical Review Letters* **130**, 221003 (2023).
- [78] V. Amitrano, A. Roggero, P. Luchi, F. Turro, L. Vespucci, and F. Pederiva, Trapped-ion quantum simulation of collective neutrino oscillations, *Physical Review D* **107**, 023007 (2023).
- [79] A. K. Jhaa and A. Chatla, Quantum studies of neutrinos on IBMQ processors, *European Physical Journal Special Topics* **231**, 141 (2022).
- [80] K. Yeter-Aydeniz, S. Bangar, G. Siopsis, and R. C. Pooser, Collective neutrino oscillations on a quantum computer, *Quantum Information Processing* **21**, 84 (2022).

- [81] M. Illa and M. J. Savage, Basic elements for simulations of standard-model physics with quantum annealers: Multigrid and clock states, *Physical Review A* **106**, 10.1103/PhysRevA.106.052605 (2022).
- [82] G. Fogli, E. Lisi, A. Marrone, and I. Tamborra, Supernova neutrino three-flavor evolution with dominant collective effects, *Journal of Cosmology and Astroparticle Physics* **2009** (04), 030.
- [83] H. Duan, G. M. Fuller, J. Carlson, and Y.-Z. Qian, Flavor Evolution of the Neutronization Neutrino Burst From an O-Ne-Mg Core-Collapse Supernova, *Physical Review Letters* **100**, 021101 (2008).
- [84] B. Dasgupta, A. Dighe, A. Mirizzi, and G. G. Raffelt, Spectral split in a prompt supernova neutrino burst: Analytic three-flavor treatment, *Physical Review D* **77**, 113007 (2008).
- [85] B. Dasgupta, A. Dighe, G. G. Raffelt, and A. Y. Smirnov, Multiple Spectral Splits of Supernova Neutrinos, *Physical Review Letters* **103**, 051105 (2009).
- [86] B. Dasgupta, A. Mirizzi, I. Tamborra, and R. Tomàs, Neutrino mass hierarchy and three-flavor spectral splits of supernova neutrinos, *Physical Review D* **81**, 093008 (2010).
- [87] A. Friedland, Self-Refraction of Supernova Neutrinos: Mixed Spectra and Three-Flavor Instabilities, *Physical Review Letters* **104**, 191102 (2010).
- [88] S. Airen, F. Capozzi, S. Chakraborty, B. Dasgupta, G. Raffelt, and T. Stirner, Normal-mode analysis for collective neutrino oscillations, *Journal of Cosmology and Astroparticle Physics* **2018** (12), 019.
- [89] M. Chakraborty and S. Chakraborty, Three flavor neutrino conversions in supernovae: slow & fast instabilities, *Journal of Cosmology and Astroparticle Physics* **2020** (01), 005.
- [90] S. Shalgar and I. Tamborra, Three flavor evolution in fast pairwise neutrino conversion, *Physical Review D* **104**, 023011 (2021).
- [91] H. Duan, G. M. Fuller, J. Carlson, and Y.-Z. Qian, Simulation of coherent nonlinear neutrino flavor transformation in the supernova environment: Correlated neutrino trajectories, *Physical Review D* **74**, 105014 (2006).
- [92] M.-R. Wu, Y.-Z. Qian, G. Martínez-Pinedo, T. Fischer, and L. Huther, Effects of neutrino oscillations on nucleosynthesis and neutrino signals for an 18  $M_{\odot}$  supernova model, *Physical Review D* **91**, 065016 (2015).
- [93] H. Duan, G. M. Fuller, J. Carlson, and Y.-Z. Qian, Simulation of coherent nonlinear neutrino flavor transformation in the supernova environment: Correlated neutrino trajectories, *Physical Review D* **74**, 105014 (2006).
- [94] A. Esteban-Pretel, A. Mirizzi, S. Pastor, R. Tomàs, G. G. Raffelt, P. D. Serpico, and G. Sigl, Role of dense matter in collective supernova neutrino transformations, *Physical Review D* **78**, 085012 (2008).
- [95] M.-R. Wu and Y.-Z. Qian, Resonances driven by a neutrino gyroscope and collective neutrino oscillations in supernovae, *Physical Review D* **84**, 045009 (2011).
- [96] G. G. Raffelt and G. Sigl, Self-induced decoherence in dense neutrino gases, *Physical Review D* **75**, 083002 (2007).
- [97] H. Duan and A. Friedland, Self-induced suppression of collective neutrino oscillations in a supernova, *Physical Review Letters* **106**, 091101 (2011).
- [98] A. Mirizzi and R. Tomàs, Multiangle effects in self-induced oscillations for different supernova neutrino fluxes, *Physical Review D* **84**, 033013 (2011).
- [99] G. Fogli, E. Lisi, A. Marrone, and A. Mirizzi, Collective neutrino flavor transitions in supernovae and the role of trajectory averaging, *Journal of Cosmology and Astroparticle Physics* **2007** (12), 010.
- [100] A. Banerjee, A. Dighe, and G. Raffelt, Linearized flavor-stability analysis of dense neutrino streams, *Physical Review D* **84**, 053013 (2011).
- [101] G. L. Fogli, E. Lisi, A. Marrone, A. Mirizzi, and I. Tamborra, Low-energy spectral features of supernova (anti)neutrinos in inverted hierarchy, *Physical Review D* **78**, 097301 (2008).
- [102] L. Wolfenstein, Neutrino Oscillations in Matter, *Physical Review D* **17**, 2369 (1978).
- [103] S. P. Mikheyev and A. Y. Smirnov, Resonance Amplification of Oscillations in Matter and Spectroscopy of Solar Neutrinos, *Soviet Journal of Nuclear Physics* **42**, 913 (1985).
- [104] S. P. Mikheev and A. Y. Smirnov, Resonance Enhancement of Oscillations in Matter and Solar Neutrino Spectroscopy, *Soviet Physics JETP* **64**, 4 (1986).
- [105] D. Lacroix, A. B. Balantekin, M. J. Cervia, A. V. Patwardhan, and P. Siwach, Role of non-Gaussian quantum fluctuations in neutrino entanglement, *Physical Review D* **106**, 123006 (2022).
- [106] Y. Pehlivan, A. B. Balantekin, and T. Kajino, Neutrino magnetic moment, CP violation, and flavor oscillations in matter, *Physical Review D* **90**, 065011 (2014).
- [107] M. J. Cervia, A. V. Patwardhan, and A. B. Balantekin, Symmetries of Hamiltonians describing systems with arbitrary spins, *International Journal of Modern Physics E* **28** (2019).
- [108] H. Duan, G. M. Fuller, and Y.-Z. Qian, Collective neutrino flavor transformation in supernovae, *Physical Review D* **74**, 123004 (2006).
- [109] S. Hannestad, G. G. Raffelt, G. Sigl, and Y. Y. Y. Wong, Self-induced conversion in dense neutrino gases: Pendulum in flavor space, *Physical Review D* **74**, 105010 (2006).
- [110] Y.-Z. Qian and G. M. Fuller, Neutrino-neutrino scattering and matter enhanced neutrino flavor transformation in supernovae, *Physical Review D* **51**, 1479 (1995).
- [111] J. Pantaleone, Neutrino oscillations at high densities, *Physics Letters B* **287**, 128 (1992).
- [112] J. Pantaleone, Dirac neutrinos in dense matter, *Physical Review D* **46**, 510 (1992).



- [113] A. Friedland and C. Lunardini, Neutrino flavor conversion in a neutrino background: Single- versus multiparticle description, *Physical Review D* **68**, 013007 (2003).
- [114] N. F. Bell, A. A. Rawlinson, and R. F. Sawyer, Speedup through entanglement: Many-body effects in neutrino processes, *Physics Letters B* **573**, 86 (2003).
- [115] R. F. Sawyer, “Classical” instabilities and “quantum” speed-up in the evolution of neutrino clouds, arXiv preprint hep-ph/0408265 (2004).
- [116] A. Friedland, B. H. J. McKellar, and I. Okuniewicz, Construction and analysis of a simplified many-body neutrino model, *Phys. Rev. D* **73**, 093002 (2006).
- [117] A. B. Balantekin and Y. Pehlivan, Neutrino–neutrino interactions and flavour mixing in dense matter, *Journal of Physics G: Nuclear and Particle Physics* **34**, 47 (2007).
- [118] L. Johns, Neutrino many-body correlations, arXiv preprint arXiv:2305.04916 (2023), arXiv:2305.04916v2 [hep-ph].
- [119] D. F. Fiorillo, G. G. Raffelt, and G. Sigl, Inhomogeneous kinetic equation for mixed neutrinos: Tracing the missing energy, arXiv **2401**, 05278v1 (2024), 10 Jan 2024.
- [120] V. Cirigliano, S. Sen, and Y. Yamauchi, Neutrino many-body flavor evolution: the full hamiltonian, (2024), arXiv:2404.16690v1 [hep-ph].
- [121] F. Capozzi, G. L. Fogli, E. Lisi, A. Marrone, D. Montanino, and A. Palazzo, Status of three-neutrino oscillation parameters, circa 2013, *Physical Review D* **89**, 093018 (2014).
- [122] Z. Maki, M. Nakagawa, and S. Sakata, Remarks on the Unified Model of Elementary Particles, *Progress of Theoretical Physics* **28**, 870 (1962).
- [123] B. Pontecorvo, Inverse beta processes and nonconservation of lepton charge, *Zhurnal Éksperimental’noĭ i Teoreticheskoi Fiziki* **34**, 247 (1957).
- [124] J. Schechter and J. W. F. Valle, Neutrino masses in  $SU(2) \times U(1)$  theories, *Physical Review D* **22**, 2227 (1980).
- [125] R. L. Workman and others (Particle Data Group), Review of Particle Physics, *Progress of Theoretical and Experimental Physics* **2022**, 083C01 (2022), <https://academic.oup.com/ptep/article-pdf/2022/8/083C01/49175539/ptac097.pdf>.
- [126] C. McGeoch and P. Farré, *Advantage Processor Overview*, Tech. Rep. 14-1058A-A (D-Wave Quantum Inc., 2022).
- [127] T. Kadowaki and H. Nishimori, Quantum annealing in the transverse Ising model, *Physical Review E* **58**, 5355 (1998).
- [128] D-Wave Systems Documentation, <https://docs.dwavesys.com/docs/latest/index.html>, accessed on December 8, 2023.
- [129] A. Lucas, Ising formulations of many NP problems, *Frontiers in Physics* **2**, 5 (2014).
- [130] J. R. McClean, J. A. Parkhill, and A. Aspuru-Guzik, Feynman’s clock, a new variational principle, and parallel-in-time quantum dynamics, *Proceedings of the National Academy of Sciences* **110**, E3901 (2013).
- [131] A. Teplukhin, B. K. Kendrick, and D. Babikov, Calculation of Molecular Vibrational Spectra on a Quantum Annealer, *Journal of Chemical Theory and Computation* **15**, 4555 (2019).
- [132] A. Teplukhin, B. K. Kendrick, and D. Babikov, Solving complex eigenvalue problems on a quantum annealer with applications to quantum scattering resonances, *Physical Chemistry Chemical Physics* **22**, 25334 (2020).
- [133] C. C. Chang, A. Gambhir, T. S. Humble, and S. Sota, Quantum annealing for systems of polynomial equations, *Scientific Reports* **9**, 1 (2019).
- [134] S. A. Rahman, R. Lewis, E. Mendicelli, and S. Powell,  $SU(2)$  lattice gauge theory on a quantum annealer, *Physical Review D* **104**, 034501 (2021).
- [135] R. C. Farrell, I. A. Chernyshev, S. J. M. Powell, N. A. Zemlevskiy, M. Ila, and M. J. Savage, Preparations for quantum simulations of quantum chromodynamics in 1+1 dimensions. I. Axial gauge, *Physical Review D* **107**, 054512 (2023).
- [136] M. V. den Nest, A. Miyake, W. Dür, and H. J. Briegel, Universal Resources for Measurement-Based Quantum Computation, *Physical Review Letters* **97**, 150504 (2006).
- [137] N. Yoran and A. J. Short, Efficient classical simulation of the approximate quantum Fourier transform, *Physical Review A* **76**, 042321 (2007).
- [138] M. V. den Nest, W. Dür, G. Vidal, and H. J. Briegel, Classical simulation versus universality in measurement-based quantum computation, *Physical Review A* **75**, 012337 (2007).
- [139] M. V. den Nest, W. Dür, A. Miyake, and H. J. Briegel, Fundamentals of universality in one-way quantum computation, *New Journal of Physics* **9**, 204 (2007).
- [140] B. Schumacher, Quantum coding, *Physical Review A* **51**, 2738 (1995).
- [141] K. Życzkowski, P. Horodecki, A. Sanpera, and M. Lewenstein, On the volume of the set of mixed entangled states, *Physical Review A* **58**, 883 (1998).
- [142] G. Vidal and R. F. Werner, Computable measure of entanglement, *Physical Review A* **65**, 032314 (2002).
- [143] N. Klco and M. J. Savage, Minimally entangled state preparation of localized wave functions on quantum computers, *Physical Review A* **102**, 012612 (2020).
- [144] A. D. King *et al.*, Quantum critical dynamics in a 5000-qubit programmable spin glass (2023),

- arXiv:2207.13800v2 [quant-ph].
- [145] R. Tanburn, E. Okada, and N. Dattani, Reducing multi-qubit interactions in adiabatic quantum computation without adding auxiliary qubits. part 1: The "deduc-reduc" method and its application to quantum factorization of numbers (2015), arXiv:1508.04816 [quant-ph].
  - [146] H. Ishikawa, Higher-order clique reduction without auxiliary variables, in *2014 IEEE Conference on Computer Vision and Pattern Recognition* (IEEE, 2014) pp. 1362–1369.
  - [147] M. Bardet, On the complexity of a gröbner basis algorithm, in *Algorithms Seminar* (2002) pp. 85–92.
  - [148] R. Dridi and H. Alghassi, Prime factorization using quantum annealing and computational algebraic geometry, *Scientific Reports* **7**, 43048 (2017).
  - [149] A. M. Ali, A. A. Farag, and G. L. Gimel'farb, Optimizing binary mrfs with higher order cliques, in *Pattern Recognition and Image Analysis* (Springer, Berlin, Heidelberg, 2008) pp. 98–111.
  - [150] R. Tanburn, O. Lunt, and N. S. Dattani, Crushing runtimes in adiabatic quantum computation with energy landscape manipulation (elm): Application to quantum factoring (2015), arXiv:1510.07420 [quant-ph].
  - [151] N. Dattani, Quadraticization in discrete optimization and quantum mechanics (2019), arXiv:1901.04405 [quant-ph].
  - [152] E. Okada, R. Tanburn, and N. S. Dattani, Reducing multi-qubit interactions in adiabatic quantum computation without adding auxiliary qubits. part 2: The "split-reduc" method and its application to quantum determination of ramsey numbers (2015), arXiv:1508.07190 [quant-ph].
  - [153] M. Anthony, E. Boros, Y. Crama, and A. Gruber, Quadratic reformulations of nonlinear binary optimization problems, *Mathematical Programming* **162**, 115 (2017).
  - [154] V. Kolmogorov and R. Zabih, What energy functions can be minimized via graph cuts?, *IEEE Transactions on Pattern Analysis and Machine Intelligence* **26**, 147 (2004).
  - [155] D. Freedman and P. Drineas, Energy minimization via graph cuts: Settling what is possible, in *2005 IEEE Computer Society Conference on Computer Vision and Pattern Recognition (CVPR'05)*, Vol. 2 (IEEE, 2005) pp. 939–946.
  - [156] H. Ishikawa, Transformation of general binary mrf minimization to the first-order case, *IEEE Transactions on Pattern Analysis and Machine Intelligence* **33**, 1234 (2011).
  - [157] M. Anthony, E. Boros, Y. Crama, and A. Gruber, Quadraticization of symmetric pseudo-boolean functions, *Discrete Applied Mathematics* **203**, 1 (2016).
  - [158] A. C. Gallagher, D. Batra, and D. Parikh, Inference for order reduction in markov random fields, in *CVPR 2011* (IEEE, 2011) pp. 1857–1864.
  - [159] A. Rocchetto, S. C. Benjamin, and Y. Li, Stabilizers as a design tool for new forms of the lechner-hauke-zoller annealer, *Science Advances* **2**, 10.1126/sciadv.1601246 (2016).
  - [160] W. Lechner, P. Hauke, and P. Zoller, A quantum annealing architecture with all-to-all connectivity from local interactions, *Science Advances* **1**, 10.1126/sciadv.1500838 (2015).
  - [161] E. Boros and A. Gruber, On quadraticization of pseudo-boolean functions (2014), arXiv:1404.6538 [math.OA].
  - [162] E. Boros, Y. Crama, and E. Rodríguez-Heck, Quadraticizations of symmetric pseudo-boolean functions: sub-linear bounds on the number of auxiliary variables, in *ISAIM* (2018).
  - [163] E. Boros, Y. Crama, and E. Rodríguez-Heck, Compact quadraticizations for pseudo-boolean functions (2018), unpublished.
  - [164] K. W. Yip, H. Xu, T. K. S. Kumar, and S. Koenig, Quadratic reformulation of nonlinear pseudo-boolean functions via the constraint composite graph, in *International Conference on Integration of Artificial Intelligence and Operations Research Techniques in Constraint Programming* (2019) pp. 643–660.
  - [165] V. Choi, Minor-embedding in adiabatic quantum computation: I. the parameter setting problem, *Quantum Information Processing* **7**, 193 (2008).
  - [166] M. Leib, P. Zoller, and W. Lechner, A transmon quantum annealer: decomposing many-body ising constraints into pair interactions (2016).
  - [167] N. Chancellor, S. Zohren, and P. A. Warburton, Circuit design for multi-body interactions in superconducting quantum annealing systems with applications to a scalable architecture, *npj Quantum Information* **3**, 21 (2017).
  - [168] N. Chancellor, S. Zohren, P. A. Warburton, S. C. Benjamin, and S. Roberts, A direct mapping of max k-sat and high order parity checks to a chimera graph, *Scientific Reports* **6**, 37107 (2016).
  - [169] M. Anthony, E. Boros, Y. Crama, and A. Gruber, Quadratic reformulations of nonlinear binary optimization problems, (2017), unpublished.
  - [170] I. G. Rosenberg, Reduction of bivalent maximization to the quadratic case, *Cahiers du Centre d'Etudes de Recherche Operationnelle* **17**, 71 (1975).
  - [171] J. D. Biamonte, Nonperturbative k-body to two-body commuting conversion hamiltonians and embedding problem instances into ising spins, *Phys. Rev. A* **77**, 052331 (2008).
  - [172] A. Perdomo, C. Truncik, I. Tubert-Brohman, G. Rose, and A. Aspuru-Guzik, Construction of model hamiltonians for adiabatic quantum computation and its application to finding low-energy conformations of lattice protein models, *Phys. Rev. A* **78**, 012320 (2008).
  - [173] Z. Bian, F. Chudak, W. G. Macready, L. Clark, and F. Gaitan, Experimental determination of ramsey numbers,

- Physical Review Letters **111**, 130505 (2013).
- [174] A. Fix, A. Gruber, E. Boros, and R. Zabih, A graph cut algorithm for higher-order markov random fields, in *2011 International Conference on Computer Vision (IEEE, 2011)* pp. 1020–1027.
- [175] G. D. las Cuevas and T. S. Cubitt, Simple universal models capture all classical spin physics, *Science* **351**, 1180 (2016).
- [176] Kahl and Strandmark, Generalized roof duality for pseudo-boolean optimization, in *International Conference on Computer Vision* (2011).
- [177] S. A. Ocko and B. Yoshida, Nonperturbative gadget for topological quantum codes, *Physical Review Letters* **107**, 250502 (2011).
- [178] Y. Subasi and C. Jarzynski, Nonperturbative embedding for highly nonlocal hamiltonians, *Physical Review A* **94**, 012342 (2016).
- [179] R. P. Feynman, Quantum mechanical computers, *Optics News* **11**, 11 (1985).
- [180] D. Nagaj, Fast universal quantum computation with railroad-switch local hamiltonians, *Journal of Mathematical Physics* **51**, 062201 (2010).
- [181] D. Nagaj, Universal two-body-hamiltonian quantum computing, *Physical Review A* **85**, 032330 (2012).
- [182] Q.-H. Duan and P.-X. Chen, Realization of universal adiabatic quantum computation with fewer physical resources, *Physical Review A* **84**, 042332 (2011).
- [183] J. Kempe, A. Kitaev, and O. Regev, The complexity of the local hamiltonian problem, *SIAM Journal on Computing* **35**, 1070 (2006).
- [184] R. Oliveira and B. M. Terhal, The complexity of quantum spin systems on a two-dimensional square lattice, *Quantum Info. Comput.* **8**, 900 (2008).
- [185] S. Bravyi, D. P. DiVincenzo, D. Loss, and B. M. Terhal, Quantum simulation of many-body hamiltonians using perturbation theory with bounded-strength interactions, *Physical Review Letters* **101**, 070503 (2008).
- [186] Y. Cao and D. Nagaj, Hamiltonian gadgets with reduced resource requirements, *Quantum Information & Computation* **15**, 1197 (2015).
- [187] S. P. Jordan and E. Farhi, Perturbative gadgets at arbitrary orders, *Physical Review A* **77**, 062329 (2008).
- [188] C. G. Brell, S. T. Flammia, S. D. Bartlett, and A. C. Doherty, Toric codes and quantum doubles from two-body hamiltonians, *New Journal of Physics* **13**, 053039 (2011).
- [189] C. Coffrin and Z. Morrell, *Quantumannealing.jl* Documentation (2022).
- [190] D. Aharonov, W. van Dam, J. Kempe, Z. Landau, S. Lloyd, and O. Regev, Adiabatic Quantum Computation Is Equivalent to Standard Quantum Computation, *SIAM Review* **50**, 755 (2008).
- [191] J. D. Biamonte and P. J. Love, Realizable Hamiltonians for universal adiabatic quantum computers, *Physical Review A* **78**, 012352 (2008).
- [192] R. Raussendorf, D. E. Browne, and H. J. Briegel, Measurement-based quantum computation on cluster states, *Physical Review A* **68**, 022312 (2003).
- [193] I. Padilla-Gay, I. Tamborra, and G. G. Raffelt, Neutrino flavor pendulum reloaded: The case of fast pairwise conversion, *Physical Review Letters* **128**, 121102 (2022).
- [194] D. F. G. Fiorillo and G. G. Raffelt, Flavor solitons in dense neutrino gases, *Physical Review D* **107**, 123024 (2023).
- [195] B. Dasgupta and M. Sen, Fast neutrino flavor conversion as oscillations in a quartic potential, *Physical Review D* **97**, 023017 (2018).
- [196] D. F. G. Fiorillo, G. G. Raffelt, and G. Sigl, Collective neutrino-antineutrino oscillations in dense neutrino environments?, *Physical Review D* **109**, 043031 (2024).
- [197] K. Grotz and H. V. Klapdor, *The Weak Interaction in Nuclear, Particle and Astrophysics* (Adam Hilger, 1990).
- [198] V. Cirigliano, G. M. Fuller, and A. Vlasenko, A new spin on neutrino quantum kinetics, *Physics Letters B* **747**, 27 (2015).
- [199] O. G. Kharlanov and P. I. Shustov, Effects of nonstandard neutrino self-interactions and magnetic moment on collective Majorana neutrino oscillations, *Physical Review D* **103**, 095004 (2021).
- [200] J. Adhikary, A. K. Alok, A. Mandal, T. Sarkar, and S. Sharma, Neutrino spin-flavour precession in magnetized white dwarf, *Journal of Physics G: Nuclear and Particle Physics* **50** (2023).
- [201] A. K. Alok, N. R. S. Chundawat, A. Mandal, and T. Sarkar, Can neutron star discriminate between Dirac and Majorana neutrinos?, arXiv preprint arXiv:2208.02239 (2022), arXiv:2208.02239 [hep-ph].
- [202] M. Srednicki, *Quantum Field Theory* (Cambridge University Press, 2007).
- [203] H. A. Bethe, G. E. Brown, J. Applegate, and J. M. Lattimer, Equation of State in the Gravitational Collapse of Stars, *Nuclear Physics A* **324**, 487 (1979).
- [204] S. Weinberg, Baryon- and Lepton-Nonconserving Processes, *Physical Review Letters* **43**, 1566 (1979).
- [205] R. C. Farrell, I. A. Chernyshev, S. J. M. Powell, N. A. Zemlevskiy, M. Illa, and M. J. Savage, Preparations for quantum simulations of quantum chromodynamics in 1 + 1 dimensions. ii. single-Baryon  $\beta$ -decay in real time, *Physical Review D* **107**, 054513 (2023).
- [206] H. Zassenhaus, Unpublished.
- [207] W. Magnus, On the exponential solution of differential equations for a linear operator, *Communications on*

- Pure and Applied Mathematics **7**, 649 (1954).
- [208] M. H. Amin *et al.*, Quantum error mitigation in quantum annealing, (2023), arXiv:2311.01306v1 [quant-ph].
  - [209] J. Gambetta, The hardware and software for the era of quantum utility is here (2023), IBM Blog.
  - [210] T. Albash and D. A. Lidar, Demonstration of a scaling advantage for a quantum annealer over simulated annealing, *Physical Review X* **8**, 031016 (2018).
  - [211] H. M. Bauza and D. A. Lidar, Scaling advantage in approximate optimization with quantum annealing, arXiv preprint arXiv:2401.07184 (2024).
  - [212] R. Ismail, A. Kakkar, and A. Dymarsky, A quantum annealing approach to minimum distance problem, arXiv preprint arXiv:2404.17703 (2024).
  - [213] F. Fornetti, A. Gnech, F. Pederiva, M. Rinaldi, A. Roggero, G. Salme, S. Scopetta, and M. Viviani, Solving the homogeneous bethe-salpeter equation with a quantum annealer, arXiv preprint arXiv:2406.18669 (2024).
  - [214] C. C. McGeoch, K. Chern, P. Farré, and A. K. King, A comment on comparing optimization on d-wave and ibm quantum processors, arXiv preprint arXiv:2406.19351 (2024).
  - [215] B. Dasgupta and M. Sen, Fast neutrino flavor conversion as oscillations in a quartic potential, *Phys. Rev. D* **97**, 023017 (2018).
  - [216] D. F. G. Fiorillo and G. G. Raffelt, Flavor solitons in dense neutrino gases, *Phys. Rev. D* **107**, 123024 (2023).
  - [217] D. F. G. Fiorillo and G. G. Raffelt, Slow and fast collective neutrino oscillations: Invariants and reciprocity, *Phys. Rev. D* **107**, 043024 (2023).
  - [218] I. Padilla-Gay, I. Tamborra, and G. G. Raffelt, Neutrino flavor pendulum reloaded: The case of fast pairwise conversion, *Phys. Rev. Lett.* **128**, 121102 (2022).
  - [219] <https://iqus.uw.edu/>.
  - [220] <https://www.lanl.gov/projects/national-security-education-center/information-science-technology/summer-schools/quantumcomputing/index.php>.
  - [221] <https://www.dwavesys.com/>.
  - [222] <https://github.com/lanl-ansi/QuantumAnnealing.jl>.